Investigation of the Relation between Compression, Relaxation, and End Losses in the Late Phases of Theta Pinch Discharges by means of a Two-dimensional MHD Computer Programme

Wolfgang Schneider

IPP 1/124 February 1972

MAX-PLANCK-INSTITUT FÜR PLASMAPHYSIK

GARCHING BEI MÜNCHEN

MAX-PLANCK-INSTITUT FÜR PLASMAPHYSIK

GARCHING BEI MÜNCHEN

Investigation of the Relation between Compression, Relaxation, and End Losses in the Late Phases of Theta Pinch Discharges by means of a Two-dimensional MHD Computer Programme

Wolfgang Schneider

IPP 1/124 February 1972

Die nachstehende Arbeit wurde im Rahmen des Vertrages zwischen dem Max-Planck-Institut für Plasmaphysik und der Europäischen Atomgemeinschaft über die Zusammenarbeit auf dem Gebiete der Plasmaphysik durchgeführt.

IPP 1/124 W.Schneider

Investigation of the Relation between Compression, Relaxation, and End Losses in the Late Phases of Theta Pinch Discharges by means of a Two-dimensional MHD Computer Programme

February 1972 (in English)

Abstract

A two-dimensional MHD model was developed for the phases after the first fast compression of theta pinch discharges. This model was tested by comparison with theoretical and experimental results; it turned out that the model aptly describes the quasistationary phases of theta pinches, i.e. it is suitable for predicting theta pinch experiments and, in particular, is an important aid for interpreting measurements.
A detailed energy balance is made to determine quantities that cannot readily be measured and to discuss the relations between various effects.
It is found that the plasma in the late phases is only adiabatically heated. The relaxation of temperature and anisotropy is discussed, particular attention being paid to interaction with heavy impurity ions and to determining the temperature of these ions from Doppler profiles of spectral lines.
Finally, on the one hand, the dominant contribution of convection to the end losses is demonstrated by means of a detailed energy balance; on the other, the relevance of thermal conduction to the axial dynamics inside the coil is explained.

I N D E X

1. Introduction

The linear theta pinch is an experimental configuration for producing plasmas of high density and temperature. Unlike the z-pinch it is less subject to dangerous instabilities during the lifetime of the plasma, which is limited mainly by the length of the compression coil.
The effects of the compression and heating of the plasma have been the subject of numerous theoretical and experimental investigations /1/ , /2/ , /3/ . Relatively fast compression leads to high energies of the ions /4/ , at first only in two degrees of freedom perpendicular to the magnetic field, i.e. the perpendicular component of the ion pressure. The parallel component of the ions changes as a result of binary collisions; this reduces the anisotropy of the ion pressure. Unlike the ions, the electrons with their different sound velocities are not shock-heated by the compression wave, but rise in temperature essentially owing to ohmic heating. In many cases, however, this resistive heating is not classical, i.e. the specific electrical resistivity according to Spitzer /5/ must be replaced by an anomalous resistivity /6/ , /7/.

So far the essential physical processes determining the behaviour of linear theta pinches have been described by several one-dimensional codes /8/ , /9/ , /10/ , which are all based more or less on the Hain-Roberts code /11/ . But the results of these models are limited by two different obstacles: for the very fast compression of low-density plasmas magneto-hydrodynamic models are not applicable; a numerical treatment that makes better allowance for shock wave phenomena /12/ provides a more useful description in this parameter regime. On the other hand, for investigations of the phases after the first implosion the plasma is strongly affected by end effects. The first attempts to describe the end losses have been 1D axial programmes /13/ , /14/ , /15/ . But a major disadvantage has been that they assumed box profiles in the radial direction. Effects arising from superposition of radial compression and axial losses could not be adequately described. The end losses influence the radial processes and hence render measurements difficult to interpret; the individual effects can no longer be decoupled.

Therefore, a two-dimensional model was designed, which starts after the first implosion phase -in order to avoid the very complicated processes occurring in this phase- but could describe the plasma behaviour in the quasistationary phases as well as possible, in particular, the axial dynamics. The MHD approximation could be used because in most cases it affords an appropriate description of the macroscopic behaviour of the plasma in the late phases of theta pinch discharges. Even in the parameter regime of relatively collisionless plasmas the MHD equations and the

transport coefficients still yield satisfactory results. The alternatives of the MHD approximation, viz. plasma simulation /16/ , /17/ or solution by direct integration of the kinetic equation /18/ are too expensive for the computers available at present.
In the model used here, the plasma is described by the quantities ϱ , $\vec{v}$, p^e , $p^i_\perp$, $p^i_\parallel$ and $\vec{B}$ as functions of the radius r, the axial distance z, and the time t. Infinite electrical conductivity is assumed, but it can be shown that this is well justified during the adiabatic phases of plasmas of fairly high temperatures. For the numerical treatment of the problem magnetic field coordinates are used, which ensures a more accurate description of the processes along the magnetic field lines, especially the heat conduction parallel to the magnetic field. A simpler two-dimensional MHD model /19/ using a coordinate system matched to the boundary conditions suggested this new approach.

The aim of this study is to investigate the behaviour of theta pinch plasmas in the phases following the first fast compression, particularly the heating of the plasma and the relaxation of the mostly anisotropic deuterons in relation to the losses at the end of the coil. The investigations are based on detailed measurements on ISAR II (and some on ISAR I), all of the results being compared with the corresponding values obtained in the two-dimensional computer programme.
The quality of the information gained by this computer code was tested beforehand by comparison with analytical models and 1D computer programmes. Apart from a brief description of the model, this comparison with theoretical results forms the essential content of chapter 2 (MHD model).
Chapter 3 (comparison of measurements and calculations) is primarily intended to demonstrate that the model properly describes the theta pinch plasma. The importance of the computer experiment for interpreting measurements is illustrated by the Doppler broadening of spectral lines.
In chapter 4 the computer experiment is then used to discuss the following problems: firstly, the relaxation of the temperature and primarily of the anisotropy are considered; that is, the question how well the coefficients used describe these processes and, in particular, how valid the model of binary collisions is. Secondly, a detailed energy balance is made to determine the influence of thermal conduction and convection on the axial dynamics and the losses at the edge of the plasma.

Some results of these investigations are not restricted to linear theta pinches, but are applicable to toroidal configurations too. In a certain sense this 2D computer experiment represents an important intermediate step towards the very elaborate 3D codes, which will be required for describing curved configurations. This, however, will only become feasible with the next computer generation.

2. Magnetohydrodynamic Model

2.1 Basic equations and coefficients

The magnetohydrodynamic (MHD) equations describe the plasma in terms of hydrodynamics and electrodynamics; that is, the plasma is regarded as a fluid subjected to electromagnetic fields /20/ . The fluid equations are obtained as a moments expansion of the Boltzmann or Fokker-Planck equation /21/ . But the equation for the n-th moment still includes the (n+1)-th moment. In order to complete the system, this next higher moment has to be determined in another way; viz. in a 13-moment approximation in the equation for the pressure tensor $\vec{\vec{P}}$ the pressure transport tensor $\vec{\vec{q}}$ is included /22/ . Under certain conditions this tensor of rank three can be contracted to a vector, namely the heat flux.

The plasma can be regarded as a fluid if the mean free path is small compared with the characteristic dimensions of the vessel.

With this rather general model as a starting point, the following simplifications are made: (1) a fully ionized plasma is assumed; (2) quasineutrality can be assumed if the characteristic frequencies are smaller than the plasma frequency or if the characteristic lengths are larger than the Debye length.
Under these conditions the two continuity equations for the electrons and ions can be combined to give an equation for the mass density ϱ . The two equations for the velocities $V^{(e)}$ and $V^{(i)}$ can be combined in any case, and so one obtains an equation for the mass velocity $\vec{V}$ and one for the current $\vec{j}$. The first equation is the equation of motion for the whole plasma, the second is the generalized Ohm's law.

In Maxwell's equations the displacement current is ignored (3) since the propagation velocity of the phenomena investigated is small relative to the light velocity.

Under certain conditions the generalized Ohm's law can be simplified (4): the inertia terms can be omitted if the frequencies remain small; if azimuthal symmetry is assumed and B_Θ is neglected, the current density $\vec{j}$ has only a Θ-component, i.e. the Hall term $\vec{j}\times\vec{B}$ only makes a contribution to the electric field strength normal to the flux surfaces; the pressure gradients are ignored since $\omega/\Omega_e \ll (V/v^e_{th})^2$, where $\Omega_e = eB/m^e c$ is the electron cyclotron frequency and v^e_{th} is the thermal velocity of the electrons); the term $m^e/m^i \nabla p^i$ can always be neglected since $m^e/m^i \ll 1$.

The most essential constraint is the assumption of infinite electrical conductivity (5) ($\sigma = \infty$) . As will be found,

however, this is an adequate approximation for the cases investigated here. This assumption not only simplifies the system of equations, it also allows a numerically effective solution method.

From assumptions (4) and (5) it follows that flux conservation is satisfied, this being expressed by Eq. (9). This yields the following system of basic equations (MDH model) for the quantities: $\{ \varrho , \vec{v}, p^e, p^i_\perp, p^i_\parallel ; \vec{E}, \vec{j}, \vec{B} \} = f(\vec{x},t)$.

Moment equations:

$$\frac{\partial}{\partial t} \varrho + \frac{\partial}{\partial x_\mu} (\varrho v^\mu) = 0 \tag{1}$$

$$\frac{\partial}{\partial t} v^\alpha + v^\mu \frac{\partial}{\partial x_\mu} v^\alpha + \frac{1}{\varrho} \frac{\partial}{\partial x_\mu} p^{\alpha\mu} - \frac{1}{\varrho} \frac{1}{c} \left[\vec{j} \times \vec{B} \right]^\alpha = 0 \tag{2}$$

$$\frac{\partial}{\partial t} p^e + v^\mu \frac{\partial}{\partial x_\mu} p^e + \frac{5}{3} p^e \frac{\partial}{\partial x_\mu} v^\mu + \frac{\partial}{\partial x_\mu} S^{(e)\mu} = \frac{1}{3} J^{ei}_{\alpha\alpha} \tag{3}$$

$$\frac{\partial}{\partial t} p^i_\perp + v^\mu \frac{\partial}{\partial x_\mu} p^i_\perp + p^i_\perp \left(2 \frac{\partial v^1}{\partial x_1} + 2 \frac{\partial v^2}{\partial x_2} + \frac{\partial v^3}{\partial x_3} \right) + \frac{\partial}{\partial x_\mu} S^{(i_\perp)\mu} = \frac{1}{2} (J^{ie}_{11} + J^{ie}_{22}) + \frac{1}{2} (J^{ii}_{11} + J^{ii}_{22}) \tag{4}$$

$$\frac{\partial}{\partial t} p^i_\parallel + v^\mu \frac{\partial}{\partial x_\mu} p^i_\parallel + p^i_\parallel \left(\frac{\partial v^1}{\partial x_1} + \frac{\partial v^2}{\partial x_2} + 3 \frac{\partial v^3}{\partial x_3} \right) + \frac{\partial}{\partial x_\mu} S^{(i_\parallel)\mu} = J^{ie}_{33} + J^{ii}_{33} \tag{5}$$

Maxwell's equations:

$$\frac{1}{c} \frac{\partial}{\partial t} \vec{B} = - \vec{\nabla} \times \vec{E} \tag{6}$$

$$\vec{j} = \frac{c}{4\pi} \vec{\nabla} \times \vec{B} \tag{7}$$

$$\vec{\nabla} \cdot \vec{B} = 0 \tag{8}$$

Ohm's law:

$$\vec{E} + \frac{1}{c} \left[\vec{v} \times \vec{B} \right] = 0 \tag{9}$$

Equation (1) is the continuity equation; the equation of motion (2) differs from the corresponding equation of hydrodynamics essentially with respect to the Lorentz force j x B. Besides containing the heat fluxes S, the pressure equations (3), (4) and (5) also include collision terms J, which describe the temperature relaxation between electrons

and ions and the relaxation of the temperature anisotropy of the ions due to binary collisions. These relaxation coefficients J and the heat fluxes S were taken from Chodura-Pohl /23/. The description of the anisotropy relaxation is equivalent to the formulation of Lehner /25/ and has already been used in a simpler form by Kogan /24/.

2.2 Initial boundary value problem

Magnetic field coordinates were used for treating the problem; compared with cylindrical coordinates, the set of surfaces r = const is replaced by surfaces of constant magnetic flux F or, to be more precise, by a function s(F) . This coordinate system is better suited to the problem since many physical phenomena occur preferentially along the magnetic field surfaces (e.g. heat fluxes). Last but not least, this is seen in a more exact numerical treatment since the numerical diffusion due to interpolation is absent.

These curvilinear coordinates are in general non-orthogonal and time dependent. With infinite electrical conductivity the plasma is tied to the field lines, i.e. the motion of the plasma normal to the field lines is described by the change of the coordinate system. This motion is given by the compression term DIVW, which occurs on transformation of the fundamental equations. The curvature of the magnetic surfaces is expressed by another term GZ.

The quantities $\vec{E}$ and $\vec{j}$ can be eliminated from the fundamental equations. The magnetic field is described by the inverse of the flux function s(r,z,t), i.e. the function R(s,z,t), where R is the radius of the flux tube s.

If azimuthal symmetry $\frac{\partial}{\partial \Theta} = 0$ is assumed and the azimuthal component of the magnetic field and the velocity ($B_\Theta = v_\Theta = 0$) are ignored, transformation of the fundamental equations (1) to (9) yields a system of differential equations for the quantities ϱ , v_z , w_s , p^e, $p'_\perp$, $p'_{\parallel}$, B_r , B_z . Here v_z is the velocity of the plasma along the field lines; the velocity v_s , i.e. the motion of the plasma relative to the magnetic field lines, vanishes owing to the assumption of infinite electrical conductivity ($\gamma = 0$); w_s is the velocity of the coordinate surfaces s = const.

The differential equation for this velocity w_s is not completely solved, i.e. with allowance for radial inertia, in all the calculations made because the necessary solution method is very time consuming. For many cases this radial dynamics is ignored, i.e. the radial plasma motion is treated as quasi-equilibrium; physically, this means that the radial oscillations are damped infinitely fast.
As the heat fluxes perpendicular to the magnetic field are

small compared with the heat fluxes parallel to the field lines, only the z-components are taken into account. The magnetic field on the coil surface was given by experimentally determined values B(t).

The initial condition for the problem is an already compressed plasma which is homogeneous in the z-direction; this plasma is given by the radial profiles of $n(r)$, $kT^e(r)$, $kT^i_\perp(r)$, $kT^i_\parallel(r)$ and the value of $B(t)$, radial equilibrium being assumed; it is also assumed that $v_z(t=t_0) = 0$ (and $w_S(t_0) = 0$).
The following boundary conditions were chosen:
a) For the magnetic field it is assumed that the coil surface is a flux tube; at the end of the coil B is continued periodically, i.e. in terms of the coordinate system:

$$\left.\frac{\partial R}{\partial z}\right|_{z=L} = 0$$

b) For the dynamic quantities Y: $\{\varrho, v_z, p^e, p^i_\perp, p^i_\parallel\}$ and the heat fluxes Y: $\{S^e_z, S^i_z, S^i_z\}$ boundary conditions were chosen which allow free outflow into the vacuum; in mathematical terms, this means linear extrapolation:

$$\left.\frac{\partial^2 Y}{\partial z^2}\right|_{z=L} = 0$$

This system of coupled partial differential equations is numerically solved by difference methods. The convergence of the numerical solution with the exact solution is generally given by the Lax-Richtmyer theorem, which states: "if the problem is consistently formulated, i.e. if the approximation is equivalent owing to finite differences of the differential equation, stability of the difference method is a necessary and sufficient condition for convergence" /26/. A detailed description of the transformation of the differential equations, the formulation of the initial boundary value problem, and its numerical solution will appear in a separate report /27/.

2.3 Additional equations for impurities

The impurities added to the deuteron plasma are generally described by a system of equations like that described above. These equations, however, are not treated in such a general way as the rest of the plasma; the impurities are to be heated only by radial adiabatic compression and interact with the plasma through binary collisions. It is assumed, moreover, that the impurities have the same macroscopic velocity V as the electrons and ions. This simplifies the description of the impurities, which can thus be characterized by three equations for the quantities ϱ^s, $p^s_\perp$, $p^s_\parallel$.

The differential equations are of the form:

$$\frac{\partial}{\partial t} \varrho^s + \varrho^s \, \mathrm{DIVW} = 0 \tag{10}$$

$$\frac{\partial}{\partial t} p_\perp^s + 2\, p_\perp^s \, \mathrm{DIVW} = \frac{1}{2}\left(J_{11}^{se} + J_{22}^{se}\right) + \frac{1}{2}\left(J_{11}^{si} + J_{22}^{si}\right) + \frac{1}{2}\left(J_{11}^{ss} + J_{22}^{ss}\right) \tag{11}$$

$$\frac{\partial}{\partial t} p_\parallel^s + p_\parallel^s \, \mathrm{DIVW} = J_{33}^{se} + J_{33}^{si} + J_{33}^{ss} \tag{12}$$

Here DIVW is the coordinate term describing the adiabatic compression. The collision terms on the RHS of the equations are again taken from Chodura-Pohl /23/; the corresponding interaction terms have to be added to the equations for the electron pressure (Eq. (3)) and for the two ion pressure components (Eqs. (4), (5)).

2.4 Testing of the model

The correctness and quality of the model were tested in a series of comparisons with analytical and simple numerical models. The result of the 2D calculation for a plasma homogeneous in the r-direction and without end losses and relaxation was compared with analytical results for adiabatic compression. Figure 1 plots for a certain magnetic field profile B(t) (dashed curve) the values calculated in the 2D code for the density n(t), electron temperature $kT^e(t)$, and the perpendicular component of the ions $kT_\perp^i(t)$ (solid curves) versus time. The corresponding analytically determined values (○, ×, ▲) are denoted by points. As the figure shows, the results of the 2D calculation agree with the analytical predictions according to

$$\Delta n(t) \sim \Delta B(t)$$

$$\Delta kT^e(t) \sim \left(\Delta B(t)\right)^{2/3}$$

$$\Delta kT_\parallel^i(t) = 0$$

$$\Delta kT_\perp^i(t) \sim \Delta B(t)$$

with an accuracy of about 1 % . This is a satisfactory approximation of the analytical formulae by the numerical calculation. The parallel component of the ion temperature remains exactly constant; this is not shown in the figure.

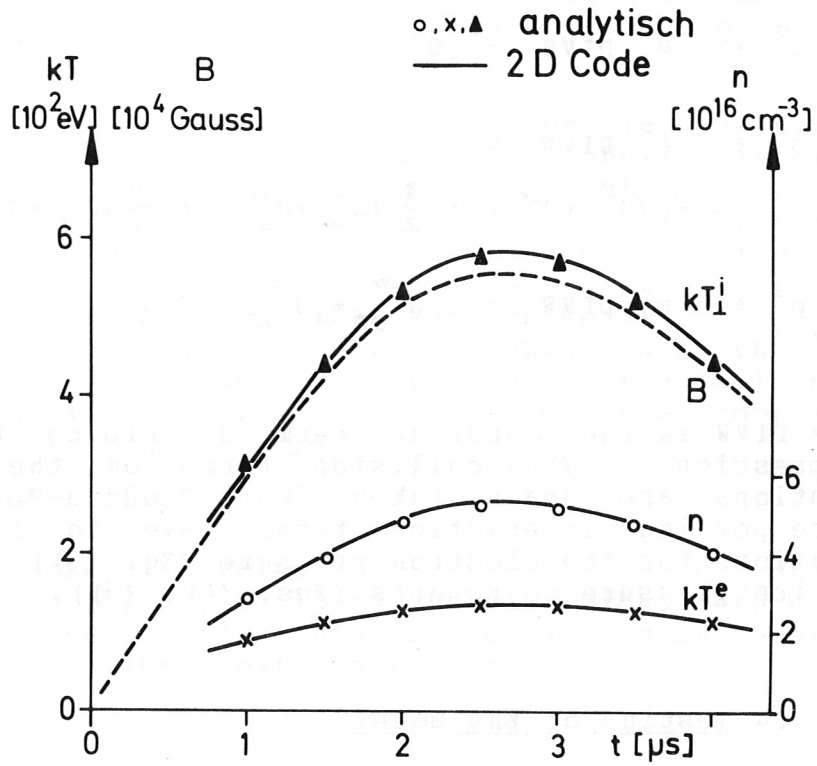

Fig. 1 Comparison of 2D code with analytic results for the adiabatic compression (2D code without relaxation and end losses).

The description of the anisotropy and primarily of the relaxation was checked by comparison with simple numerical calculations of Lehner, Neuhauser, and Pohl /28/ . The curves given by Lehner-Pohl in /29/ for the relaxation of heavy impurity ions in an anisotropic deuteron plasma were compared with results of the 2D code (without compression and end losses). The curves given by Lehner-Pohl in /29/ for the relaxation of heavy impurity ions in an anisotropic deuteron plasma were compared with results of the 2D code (without compression and end losses). The results of this comparison is shown in Fig. 2. The solid curves show the results of the 2D code; the values of Lehner-Pohl are denoted by points (O,●,Δ,▲,x). This comparison, too, is completely satisfactory. In a certain sense this is also a comparative test of the coefficients given by Lehner /25/ and those by Chodura/Pohl /23/ for the relaxation of the anisotropy and temperature. The two formulations differ appreciably but yield the same results, as the test shows.

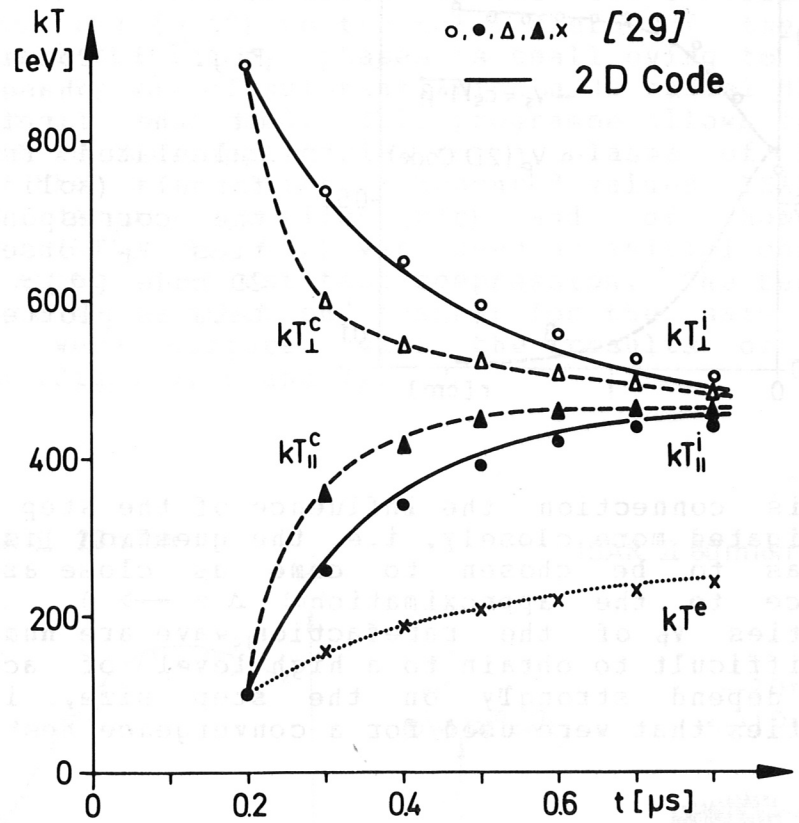

Fig. 2 Comparison of 2D code, with respect to relaxation of temperature and anisotropy (of heavy impurity ions as well), with results of Lehner-Pohl.

The axial behaviour of the 2D programme (one-fluid model without thermal conduction) was compared with results of J.Wesson /30/ . According to Wesson's theory the velocity of the rarefaction wave due to the end losses is equal to the sound velocity times $\sqrt{1-\beta}$. This result of Wesson was checked with the 2D code for every flux tube and satisfactory agreement was obtained. Wesson's model treats a radial box-shaped profile; the comparison should therefore be correct for every single flux tube. In Fig. 3 the velocity v_s is plotted for fixed z and t versus the radius. Here the velocities V_p of the rarefaction wave observed in the 2D calculations were plotted for various flux tubes. The agreement is satisfactory.

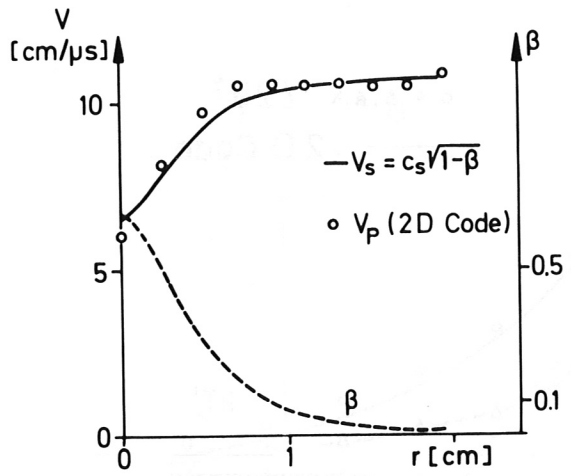

Fig. 3 Comparison of phase velocities of the rarefaction wave calculated from Wesson's formula (solid curve) and the corresponding velocities V_P observed in the 2D code ($\circ$); in addition, beta is plotted (dashed).

In this connection the influence of the step size Δz was investigated more closely, i.e. the question is how small Δz has to be chosen to come as close as possible in practice to the approximation $\Delta z \longrightarrow 0$. As these velocities V_P of the rarefaction wave are numerically the most difficult to obtain to a high level of accuracy, and hence depend strongly on the step size, it was these quantities that were used for a convergence test.

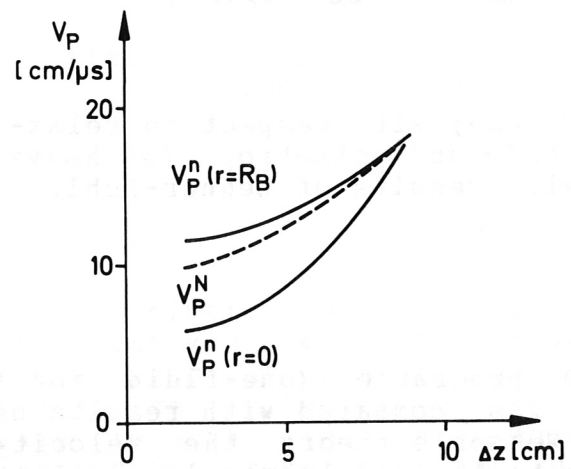

Fig. 4 Convergence of the phase velocities of the rarefaction wave in the 2D code.

Figure 4 shows the convergence of these wave velocities as observed on the density on the axis V^n_P (r=0), the density at the plasma boundary V^n_P (r=R_B), and from the line density V^N_P. With a step size of $\Delta z \approx 2$ cm, which is roughly equivalent to fifty mesh points over a length of 100 cm in the z-direction, the approximation is already quite good for these velocities. The convergence shown is in agreement with the Lax-Richtmyer theorem /26/ because the numerical methods for solving the problem yielded stability.

For the model treated here infinite conductivity is assumed ($\eta = 0$) (Sec. 2.1), i.e. the ohmic heating of the electrons is neglected. It can be estimated that the contribution of the ohmic heating (ηj^2) to the total energy of the plasma in the quasi-stationary phases is small owing to the high temperature. By way of substantiation a 1D radial MHD model of H. Fisser /10/ was used. This programme allows for ohmic heating, but is only applicable to a plasma of infinite extent in the z-direction. Measured values (ISAR II and ISAR I) of density profiles n(r) and of homogeneous temperatures (kT^e, kT_i, kT_n) were used as initial conditions at a time after the first fast compression. The results of the 2D programme (without end losses) for the same initial conditions were compared with the results of the 1D calculation (Figs. 5, 6 and 7).

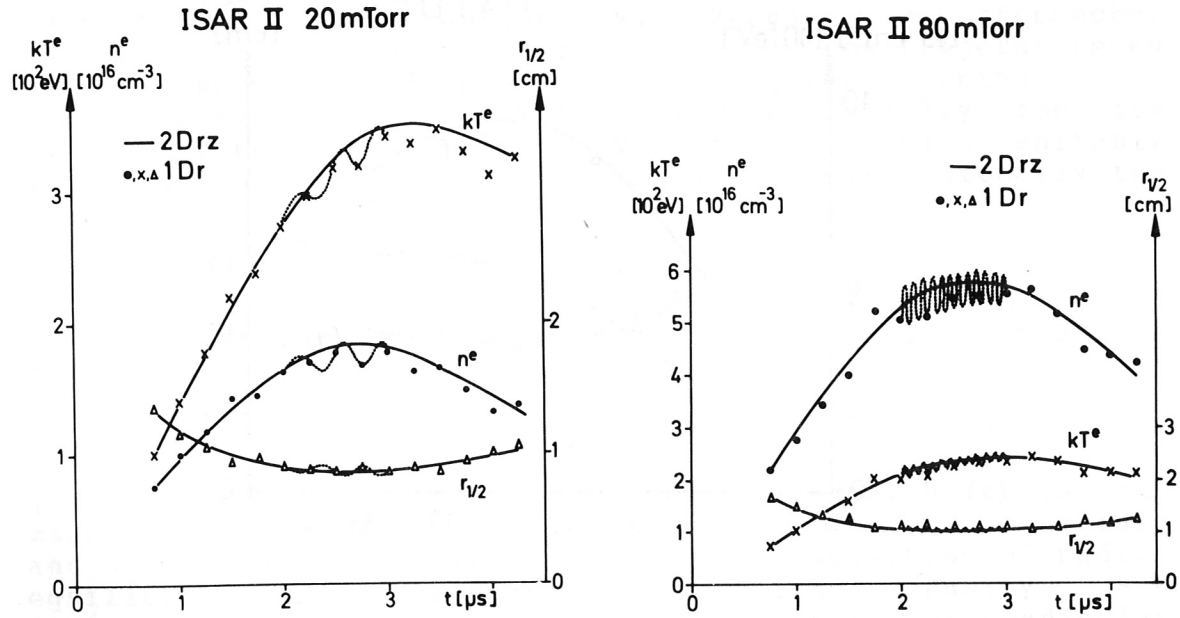

Fig. 5,6 Comparison between 1D(r) code and 2D(r,z) code with reference to electron temperature and density and to the half-radius of the density profiles (ISAR II, 20 and 80 mTorr D_2).

In each case the electron temperature kT^e and electron density n in the centre of the coil and the half-widths $r_{1/2}$ of the radial density profiles in the midplane of the discharge vessel are plotted. For clarity, only the results of the 2D code were plotted in curve form, the results of the 1D programme being plotted for individual times only. The reason why the results of the 1D calculation do not always coincide with those of the 2D calculation is that the

1D programme makes full allowance for the radial inertia, i.e. it oscillates about the equilibrium. This is indicated in a few figures for one time interval. The 2D programme was used here on the assumption of quasi-equilibrium, i.e. these radial oscillations were damped. As the figures confirm, the different descriptions of the radial behaviour in the two codes (1Dr: $\nu > 0$; 2Drz: $\nu = 0$) lead to the same results, i.e. the ohmic heating is negligible relative to the adiabatic compression.

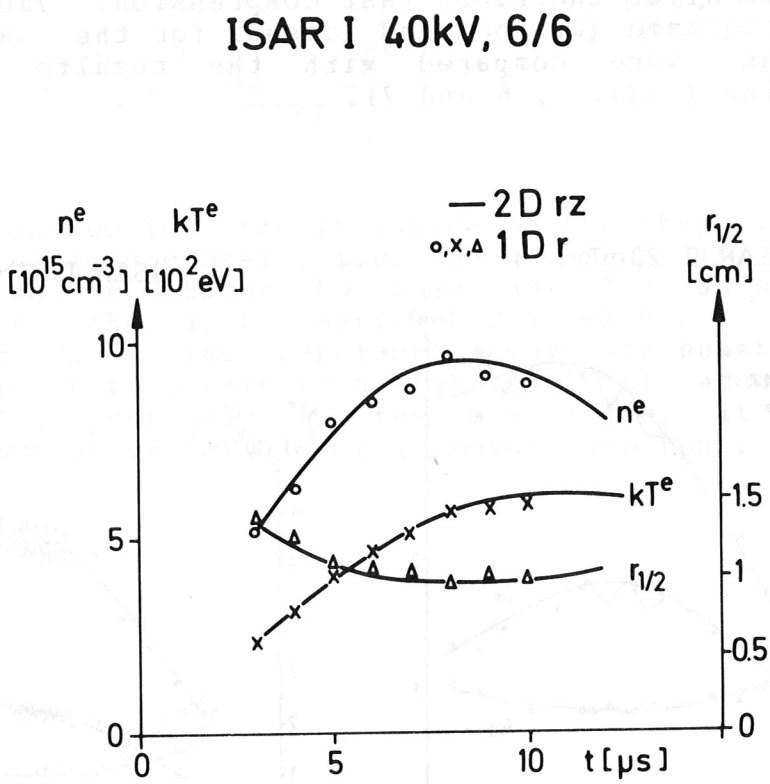

Fig. 7 Comparison between 1D(r) code and 2D(r,z) code with reference to electron temperature and density and to the half-radius of the density profiles (ISAR I; 5.40 m coil).

Since, on the other hand, the agreement between experiment and calculation is satisfactory, as is shown in Chapter 3, it can be concluded that nor do anomalous resistive heating or anomalous diffusion occur. It has already been shown /7/, /31/ that the plasma in the quasi-stationary phases can be described in terms of classical electrical conductivity, and that no anomaly is observed. In the cases discussed here, however, the classical ohmic heating is so small owing to the high temperatures that it can be neglected relative to the magnetic field compression.

3. Comparison between Experiment and Model

3.1 Measuring methods

The experiments were carried out on the ISAR II 500 kJoule linear theta pinch bank with a double-fed coil of 1 m length and 10 cm in diameter. The plasma diameter was about 2 cm in the late phases. Typical discharge conditions were at 25 kV charging voltage: $\dot{B} = 3 \times 10^{10}$ Gauss/sec and a maximum field B = 52 kGauss. The measurements used for comparison were concentrated on two filling pressures of 20 and 80 mTorr deuterium /32/ . The low filling pressure guaranteed high anisotropic ion temperatures and rather slow relaxation of particle energies, while the higher filling pressure served for a discussion of a faster relaxing and more isotropic plasma. The electron density was determined from side-on radially resolved measurements of the emission coefficients of the free-free continuum radiation around 5300 Å and from end-on Mach-Zehnder interferometer measurements in the visible. The electron temperature on the axis was obtained from 90° laser light scattering.
The diamagnetic flux, which yields essentially the ion energy within the plasma, was measured with suitably arranged loops /33/. The test signal ϕ_s gives directly the flux displaced by the plasma:

$$\phi_s = 2\pi \int_0^{R_p} (B_a - B_i(r)) \; r \, dr \; .$$

This displaced flux is related to the total flux in the coil without plasma as follows:

$$\Delta\phi = \frac{\phi_s}{\phi_{vac}} = \frac{\phi_s}{\pi R_c^2 B_a}$$

(B_a is the magnetic field outside the plasma, $B_i(r)$ is the magnetic field within the plasma, R_p is the plasma radius, and R_c is the coil radius). Under the assumption of radial equilibrium and knowledge of the line density $N = 2\pi \int n(r) \, r \, dr$ it is possible to obtain the perpendicular energy of the plasma from the diamagnetic signal:

$$kT_\perp = \frac{1}{8\pi} \left(1 + \sqrt{1 - \beta} \right) \frac{R_c \phi_s}{N}$$

From this data and the known electron temperature kT_e the perpendicular ion energy can be calculated.

A scintillator together with a multiplier -absolutely calibrated with a silver counter- allowed the neutron flux rate to be measured. What is measured here is the total number of neutrons per unit time that are emitted in the D-D reaction $D + D \longrightarrow He_3 + n$. The cross section for this reaction is a function of the mean ion energy (for various energy distribution functions of the ions). The mean ion energy can thus be determined from the neutron flux in conjunction with the density distribution.

3.2 Comparison of the experimentally determined plasma parameters with results of the model

These measurements were compared with the two-dimensional calculations started at t_o = 0.75 μsec with experimental data. To be more precise, the initial conditions for the computer code were the experimentally determined radial density profile $n(r,t_o)$ and the electron temperature measured in the coil centre $kT^e(t_o)$ together with the measured vacuum magnetic field $B(t_o)$. The perpendicular ion temperature $kT_\perp^i(t_o)$ was estimated from the diamagnetic signal, and the parallel ion temperature $kT_\parallel^i(t_o)$ was assumed to be approximately equal to the electron temperature. All temperatures were assumed to be uniform over the radius at time $t = t_o$; furthermore, the initial conditions were homogeneous in the axial direction; the velocity $V(t_o)$ was set equal to zero.

Fig. 8 shows a comparison between the solutions of the computer programme (represented in curve form) and the

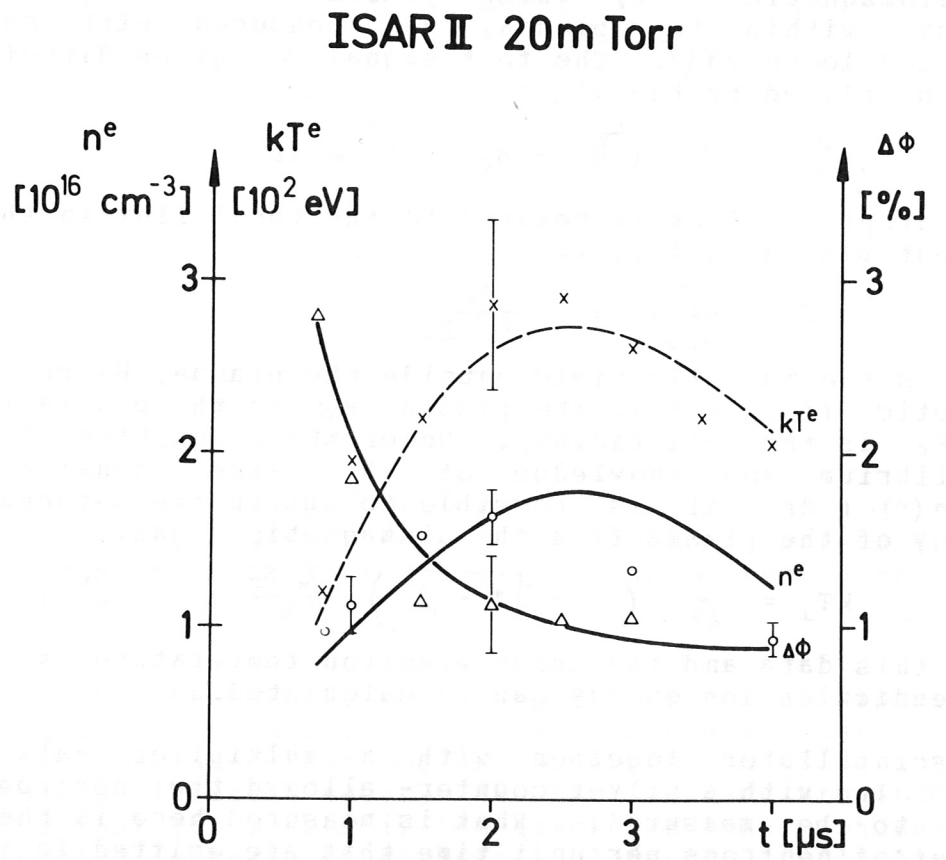

Fig. 8 Comparison of the measured electron temperature (×), electron density (○), and diamagnetic signal (△) with results of the 2D code (curves) in the 20 mTorr case.

corresponding measured values (represented as × , ○ , △), namely the electron temperature kT^e, the electron density n on the axis, and the diamagnetic signal at the midplane as a function of time for a filling pressure of 20 mTorr. In Fig. 9 the same quantities are compared for the 80 mTorr case. The calculated values agree well within the margins of error.

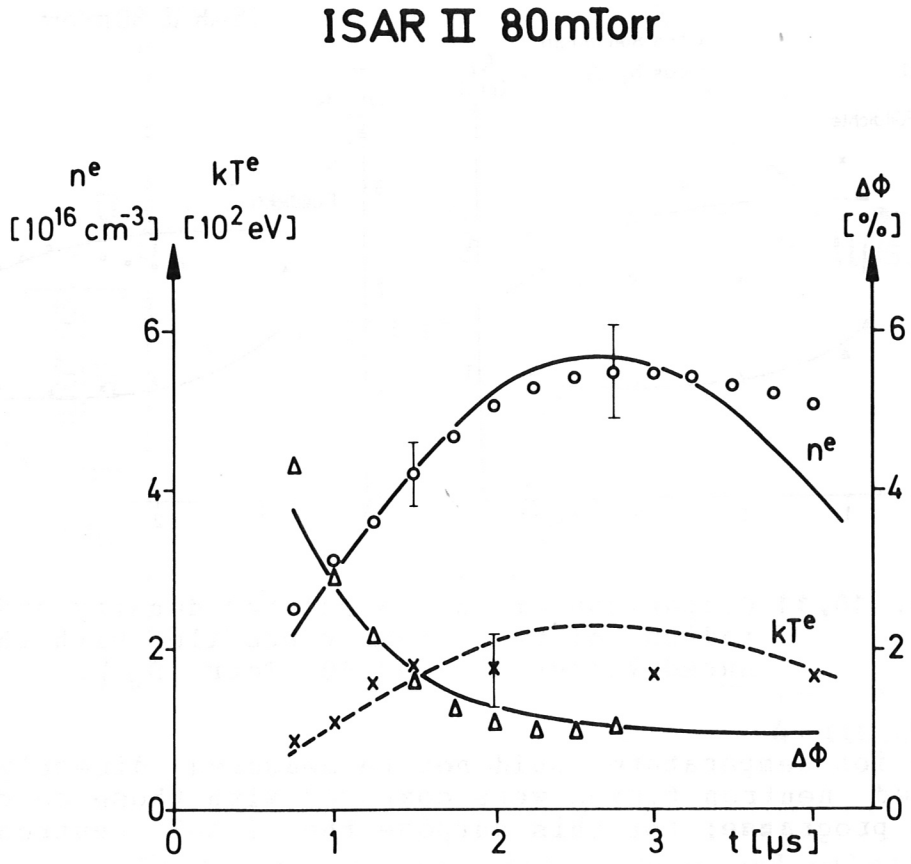

Fig. 9 Comparison of the measured electron temperature (×), electron density (○), and diamagnetic signal (△) with results of the 2D code (curves) in the 80 mTorr case.

Besides these quantities calculated directly in the programme, such secondary quantities as the plasma beta $\beta = p/(B^2/8\pi)$ the line density N, and the half-width of the radial density profiles in the midplane of the coil were compared. The comparison between calculation and measurement for the line density and half-radius are shown in Fig. 10 for the 20 mTorr case and in Fig. 11 for the 80 mTorr case. The various test points for the line density

originate from different evaluation methods: firstly, N was determined from the total particle number N_{tot} divided by the length of the plasma (symbol o); the other test points (×) derive from the evaluation of the continuum radiation.

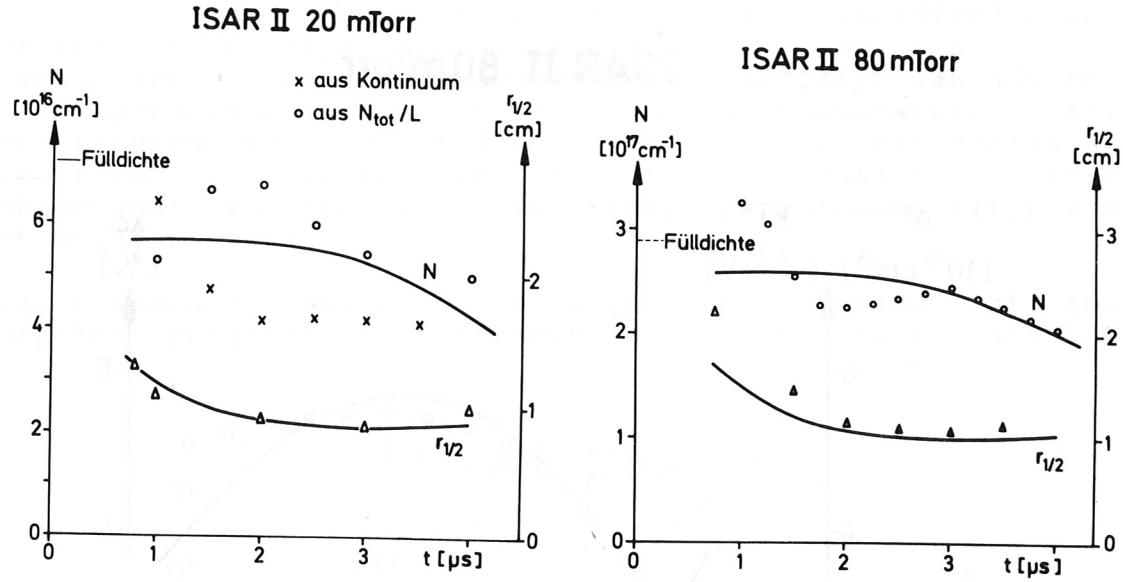

Fig. 10,11 Comparison of the calculated density and half-radius of the density profile with the measured values (20 and 80 mTorr D_2).

As the ion temperature could not be measured directly, the measured neutron fluxes were compared with those calculated in the programme; for this purpose the local neutron flux rate

$$R = 1/2\ n^2 \langle \sigma_q \rangle$$

was integrated over the entire plasma column:

$$\dot{N}\ (t) = 2\pi \int_{-L}^{L} \int_{0}^{R_R} R(r,z,t)\ r\ dr\ dz$$

This comparison is shown in Fig. 12. The agreement between measurement and calculation is again satisfactory, particularly if it is borne in mind that the D-D reaction cross section /34/

$$\langle \sigma_q \rangle = 1.3 \times 10^{-12}\ T^{-2/3}\ \exp(-187.6\ T^{-1/3})$$

(where $T\ [eV] = 1/3\ T_{\parallel}^{i} + 2/3\ T_{\perp}^{i}$) is a steep function of temperature for deuterons of a few keV.

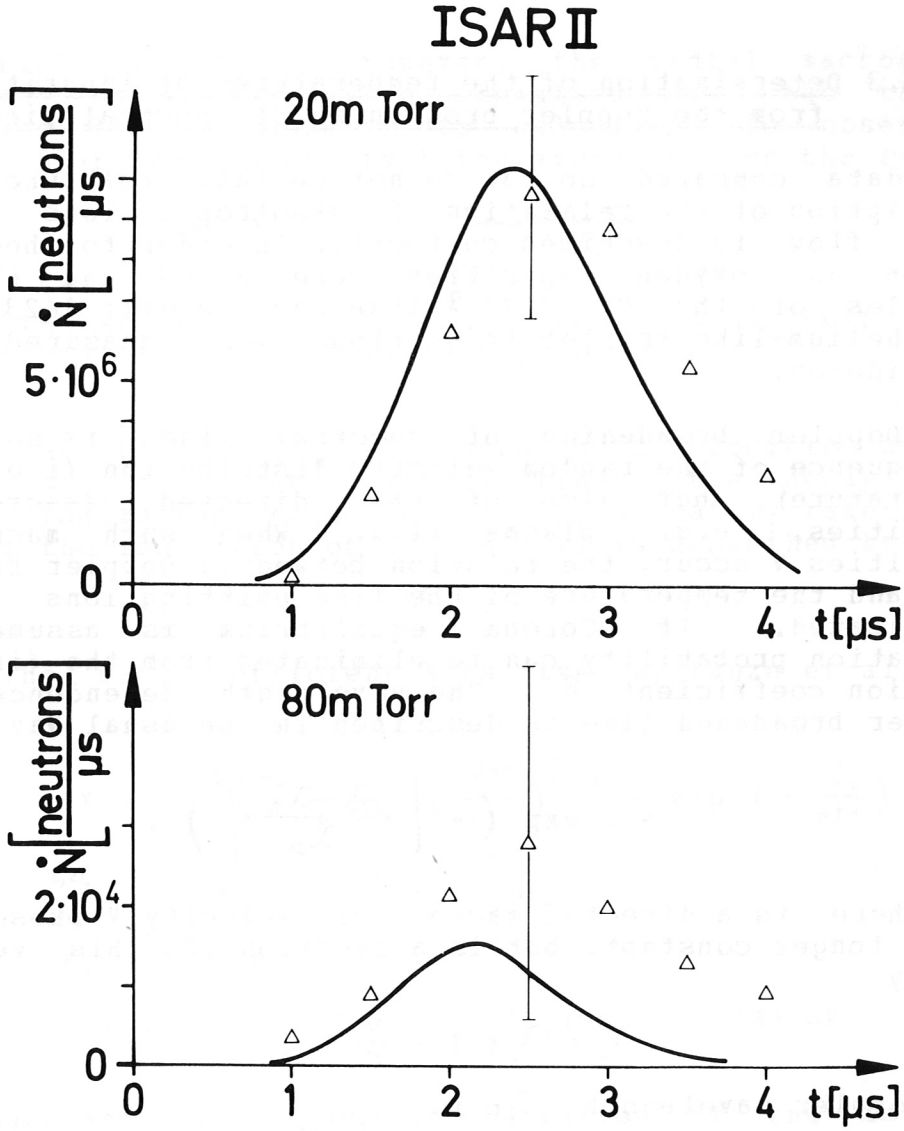

Fig. 12 Comparison between measurement and calculation for the neutron fluxes (Δ experimental points; the curves show the results of the 2D code).

At this point some remark should be made about the comparison of the calculated radial density profiles and those determined from continuum measurements. In many cases no agreement could be achieved with these density profiles. Only when the calculations were started with narrower profiles (narrower than the observed ones) was agreement obtained for later times. The suspicion that the continuum measurements at early times often yield profiles that are too wide is supported by other observations. For example, laser measurements of the density profiles at these early times yield smaller half-widths than the continuum measurements; however, the accuracy of these measurements is not yet high enough to allow a definite conclusion.

3.3 Determination of the temperatures of impurity ions from the Doppler broadening of spectral lines

The data compared so far do not reliably tell whether the description of the relaxation of anisotropic ions and the axial flow is described correctly. In order to check this, carbon and oxygen impurities were added and the line profiles of the CV 2271 Å line and the OVII 1623 Å line, both helium-like triplet transitions, were measured end-on and side-on.

The Doppler broadening of spectral lines is not only a consequence of the random velocity distribution (i.e. of the temperature), but also of the directed (macroscopic) velocities, e.g. plasma flow. When such macroscopic velocities V occur, the relation between a Doppler broadened line and the temperature of the line emitting ions is more complicated. If Corona equilibrium is assumed, the excitation probability can be eliminated from the (integral) emission coefficient ε. The wavelength dependence of a Doppler broadened line is described in the usual way /35/ by

$$\exp\left(-\left[\frac{\lambda-\lambda_o}{\lambda_D}\right]^2\right).$$

If there is a directed macroscopic velocity V present, λ_o is no longer constant, but is a function of this velocity, namely

$$\lambda_o = \lambda_o'\left(1-\frac{V}{c}\right);$$

the Doppler wavelength λ_D is

$$\lambda_D = \left(\frac{2kT_{\parallel}^s\,\lambda_o'^2}{m^s c^2}\right)^{1/2}.$$

Integration over the emission coefficient $\varepsilon(\lambda,r,z)$ in the direction of observation yields the intensity in optically thin media. The radiation power per solid angle $P(\lambda)$ recorded by the monochromator is finally obtained by further integration over the surface:

$$P(\lambda) = 2\pi\int_0^{R_B}\left(\int_{-L}^{+L}\varepsilon(\lambda,r,z)\,dz\right) r\,dr.$$

This yields the 1/e width of the end-on Doppler profile and also a formal (apparent) "Doppler temperature":

$$\langle kT_{\parallel}^s\rangle_{Doppler} = \frac{m^s c^2}{2}\left(\frac{\Delta\lambda}{\lambda_o'}\right)^2.$$

For the comparison with the experimental values of the perpendicular temperature obtained from side-on observation of the radial Doppler profiles one really ought to use the

same formalism. Since, however, the radial macroscopic velocities are negligible relative to the thermal velocities, it is possible to calculate the observable perpendicular temperature by being averaged over the radius:

$$\langle kT_\perp^s \rangle = \frac{\langle (n^s)^2 kT_\perp^s \rangle_r}{\langle (n^s)^2 \rangle_r}$$

(This is valid only after the radial compression oscillations have been sufficiently damped.)

Besides this influence of the macroscopic velocities on the Doppler broadening of spectral lines, the decay of the relevant ionization stage was also approximately taken into account; the ionization of C V to C VI is described by

$$\frac{\partial}{\partial t} n^s = - n^s n^e X$$

where the rate coefficient X is given by Kunze et al. /36/ as

$$X = 17 \frac{t_1 a_0}{m^e} \frac{1}{(1+Z)^2} \left(\frac{kT^e}{E_H} \right)^{1/2} \frac{E_H}{E_1 + kT^e} \exp \left(- \frac{E_1}{kT^e} \right)$$

$$\frac{t_1 a_0}{m^e} = 6.14 \times 10^{-9} \text{ cm}^{-3}/\text{sec}$$

$$E_H = 13.6 \text{ eV}$$

$$E_1 (\text{CV}) = 392 \text{ eV} \qquad \langle E_1 (\text{OVII}) = 739 \text{ eV} \rangle$$

This space and time dependent variation of the impurity concentration is essential for the intensity of the emitted line. As the impurity ions are further ionized faster in the hotter, denser regions of the coil centre, the end regions with higher axial velocities have greater weight in the integration of the emission coefficient ε.

The comparison of the measurements with the temperatures calculated in this way is shown in the next figures (Figs. 13, 14, and 15).

Interpretation:
The solid curves in Fig. 13 represent the perpendicular and parallel temperatures, determined by integrating the differential equations (10), (11), and (12), for the impurities in the centre of the coil as functions of time. The dotted lines are the corresponding temperatures calculated from Doppler-profiles within the code; i.e. these quantities (especially the axial one) represent both thermal and flow velocities. For comparison, the perpendicular (o)

and parallel (▲) "temperatures" obtained from end-on and side-on measurements of the Doppler profiles are also plotted. The measured and calculated axial "Doppler temperatures" agree very well in this 80 mTorr case and differ clearly from the actual parallel temperature $kT^c_{//}(r=0,z=0)$. This difference is due to the influence of the axial plasma velocity distribution on the Doppler broadening observable end-on, and hence to an apparent "Doppler temperature" $\langle kT^c_{//}\rangle_{Doppler}$. The contribution of this velocity to the Doppler broadening is at times a factor of 4 - 5 as large as that of the parallel temperature itself.

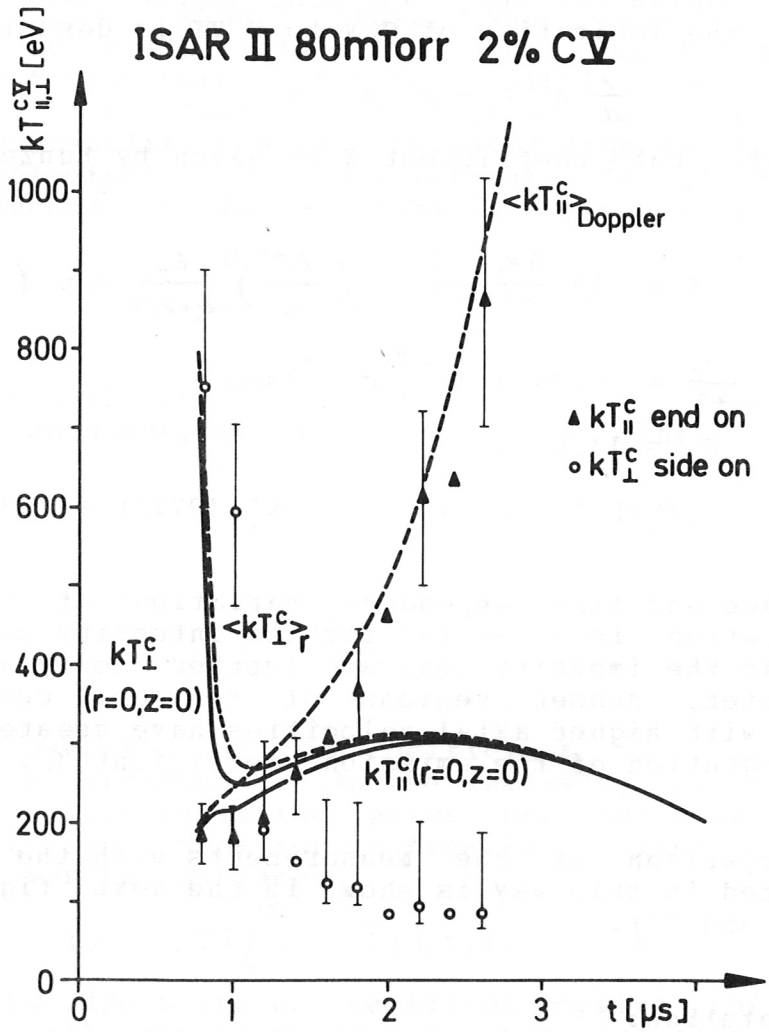

Fig. 13 Calculated actual perpendicular and parallel temperatures of impurities in the coil centre (solid curves) and comparison of apparent temperatures determined from Doppler profiles observed end-on (▲) and side-on (○) with temperatures $\langle kT^c\rangle$ calculated from actual temperatures and flow velocity (dashed curves).

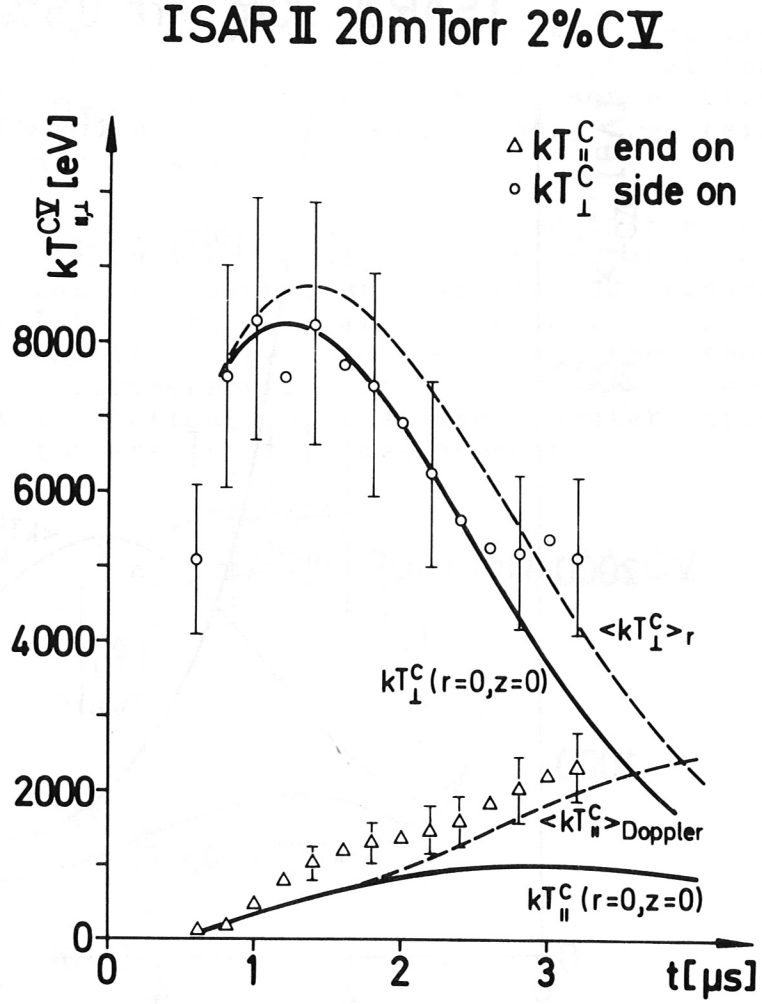

Fig. 14 Calculated actual perpendicular and parallel temperatures of impurities in the coil centre (solid curves) and comparison of apparent temperatures determined from Doppler profiles observed end-on (△) and side-on (○) with temperatures $\langle kT^{\circ}\rangle$ calculated from actual temperatures and flow velocity (dashed curves).

In the 20 mTorr case (Fig. 14) the parallel temperature and the temperature obtained by Doppler broadening differ by a factor of 2. The agreement between measurement and calculation as regards the apparent parallel temperature is not so optimum as in the higher density case because microscopic instabilities, viz. mirror instabilities, are present and cause additional relaxation /40/. In Fig. 15 the influence of this additional relaxation on the parallel temperature of O VII is even more pronounced.

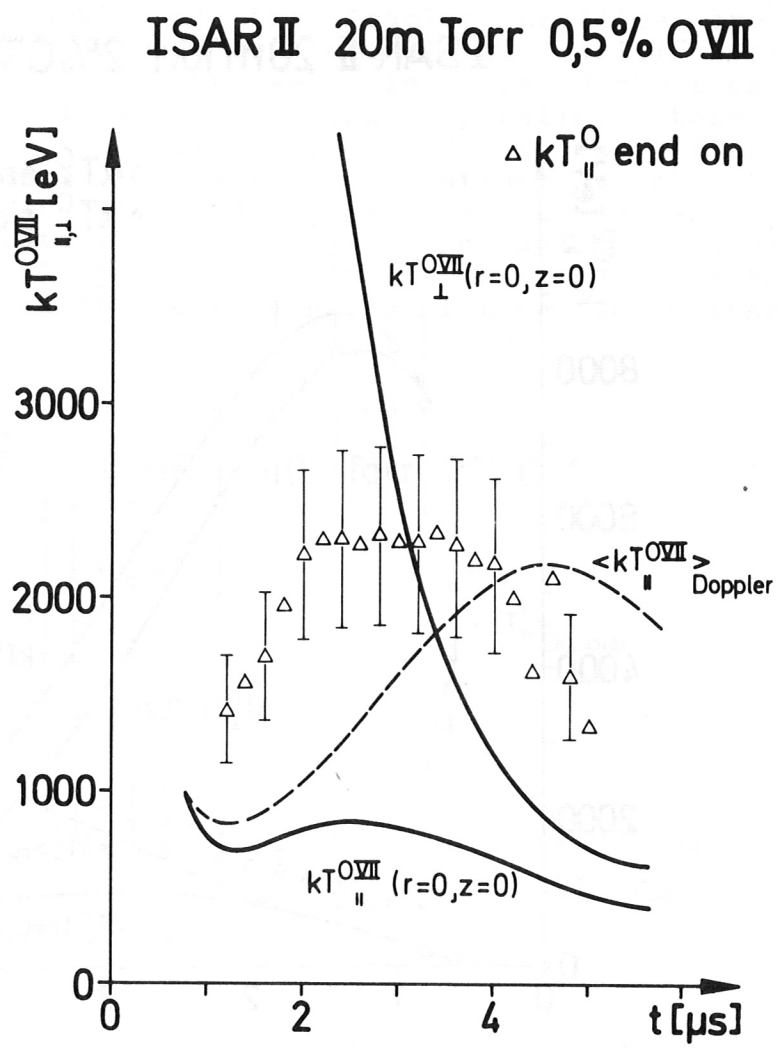

Fig. 15 Calculated actual perpendicular and parallel temperatures of impurities in the coil centre (solid curves) and comparison of apparent temperatures determined from Doppler profiles observed end-on (△) with temperature <kT$_{\parallel}^{O}$> calculated from the actual temperature and flow velocity (dashed curve).

It has thus been convincingly demonstrated that measurement of the parallel temperature of the impurities by end-on observation of the Doppler profiles without taking into account the axial plasma flow may lead to wrong results.

3.4 Result of the comparison

In Chapter 2 it was shown that the computer experiment used here yields the same results as analytical formulae or simple numerical models. In a certain sense this was a comparison with theoretical predictions, i.e. relating the 2D code to other plasma models.

The comparison of all quantities measured in the experiment with the corresponding results of the computer code showed such good agreement (Chapter 3) that the 2D programme can now be related to actual experiments: the computer experiment describes the phenomena in the theta pinch correctly. Furthermore, it has been demonstrated particularly in Section 3.3, that the computer experiment is a useful aid for interpreting measurements.

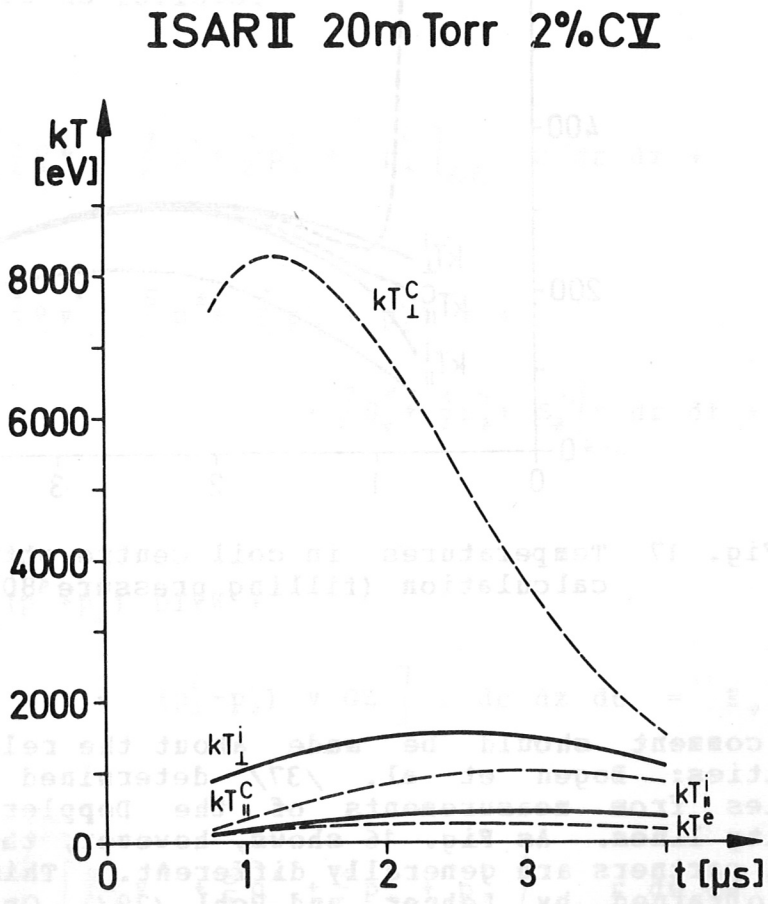

Fig. 16 Temperatures in coil centre obtained in 2D calculation (filling pressure 20 mTorr D_2).

Finally, the calculations yield the temperatures of all partners; see Figs. 16 and 17 (where the temperatures in the

coil centre are plotted as functions of time). These two plots clearly show the different relaxation behaviour in the different parameter regions of 20 and 80 mTorr filling pressure.

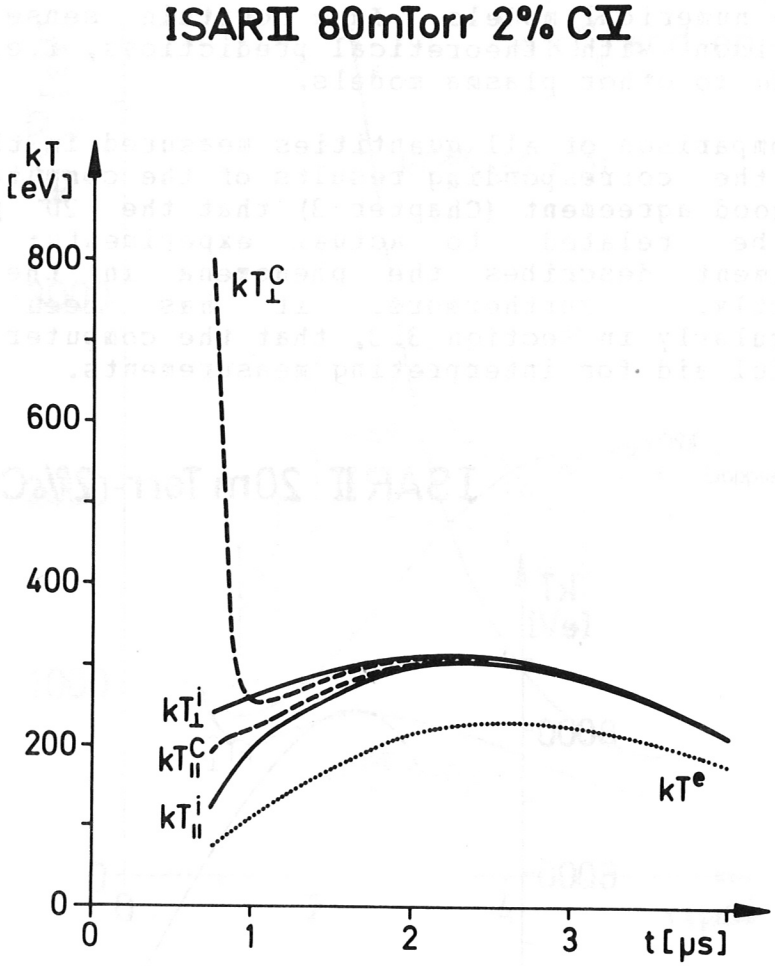

Fig. 17 Temperatures in coil centre obtained in 2D calculation (filling pressure 80 mTorr D_2).

Some comment should be made about the relaxation of the impurities: Bogen et al. /37/ determined the deuteron energies from measurements of the Doppler broadening of impurity lines. As Fig. 16 shows, however, the temperatures of all partners are generally different. This result was also obtained by Lehner and Pohl /29/. Only in cases of high density and relatively low temperatures can equality of the temperatures of deuterons and impurities be assumed (see Fig. 17).

4. Discussion of the Energy Balance

4.1 Energy balance: computation of experimentally inaccessible quantities

Once satisfactory agreement had been obtained by comparing all experimentally acessible plasma parameters with those calculated in the computer programme it was safe to discuss the data of the code without direct relation to experimental measurements. This included a detailed energy balance, i.e. a discussion of the individual energy components in the plasma (kinetic and thermal energy) and the various energy losses at the end of the coil (kinetic energy losses, energy loss by convection and thermal conduction) compared with the energy gain due to adiabatic compression.

The energy balance follows from the continuity equation, the equation of motion and the pressure equations and is written in integral form as follows:

$$2\pi \int_0^{L} \int_0^{R_B} \left[\tfrac{1}{2} \rho v^2 + \tfrac{3}{2} p^e + \tfrac{1}{2} p_{\parallel}^i + p_{\perp}^i \right]_{t=t_1} r \, dr \, dz +$$

$$+ 2\pi \int_{t_0}^{t_1} \int_0^{R_B} \Big[\left(\tfrac{1}{2} \rho v^2 + \tfrac{5}{2} p^e + \tfrac{3}{2} p_{\parallel}^i + p_{\perp}^i \right) v +$$

$$+ \tfrac{3}{2} S_z^e + \tfrac{1}{2} S_z^{i_\parallel} + S_z^{i_\perp} \Big]_{z=L} r \, dr \, dt +$$

$$+ 2\pi \int_{t_0}^{t_1} \int_0^{R_B} \int_0^{L} \Big[(p^e + p_{\perp}^i) \, \mathrm{DIVW} +$$

$$+ (p_{\perp}^i - p_{\parallel}^i) \, v \, GZ \Big] r \, dr \, dz \, dt = E_0 .$$

$$E_0 := 2\pi \int_0^{L} \int_0^{R_B} \left[\tfrac{1}{2} \rho v^2 + \tfrac{3}{2} p^e + \tfrac{1}{2} p_{\parallel}^i + p_{\perp}^i \right]_{t=t_0} r \, dr \, dz$$

is the total energy of the plasma at the start of the calculation ($t = t_0$). The first integral gives the total energy E of the plasma in the coil at the time t_1. The second integral gives the total energy losses ΔE at the

end up to the time t_1. The first part of the third integral represents the energy gain of the plasma due to adiabatic compression and is referred to in the following as ΔE_B. The second part of this integral is interpreted as the work required to change the curvature of the field lines. This energy component was so small in all the cases investigated that it will not be considered further in the following.

The total energy loss ΔE was normalized to the energy $E^* := E + \Delta E$, i.e. the energy that the plasma would have if not subject to end losses. It was thus possible to make a direct comparison of these normalized end losses $\Delta e = \Delta E / E^*$ for various cases.

The energy conservation was also checked:

$$\delta E := \left| E(t=t_0) + \Delta E_B - E^* \right| / E^* .$$

Along with the corresponding symbol δm for the mass conservation, this is a measure of the quality of the computation. In all of them the mass conservation was $\delta m \leq 1\%$; the characteristic values of δe were between 3 and 5%. Not only were the various components of the energy in the plasma $E := E_{kin} + E_P$ calculated seperately, but also the various components of the energy loss $\Delta E := \Delta E_{kin} + \Delta E_P + \Delta E_S$ and the energy gain of the plasma due to compression of the magnetic field ΔE_B. The energy terms for every plasma component (electrons, ions perpendicular and parallel) were almost all calculated separately; and, finally, the energies that are transferred from one component to the other as a result of relaxation are integrated. This yields a vast amount of data, and so here only a few aspects can be singled out for attention.

4.2 Analysis of the energy balance: convection as the dominant loss mechanism

The various energy components cannot readily be measured in a conventional experiment. Furthermore, the computer experiment can quantitatively determine the influence of certain effects ,e.g. thermal conduction, in the form of energy components.

In the following it is attempted to represent the individual energy components from various viewpoints. The two cases of 20 and 80 mTorr filling pressure in ISAR II are taken as a basis.

To give an overall picture, first the total energies for the two filling pressures are plotted in Fig. 18. Then the energy gain of the plasma due to magnetic field compression is compared in the two cases (Fig. 19). The splitting of this energy gain and of the internal energy into the various

fluid components is represented (Figs. 19 and 20). Finally, the various mechanisms composing the energy losses are discussed (Figs. 21 and 22).

a) Total energies:

In Fig. 18 the total energy of the plasma (E) and the total energy losses (Δ E) at the end of the coil are plotted for the two filling pressures (these values are valid absolutely for half the coil in each case). Also plotted is the virtual plasma energy (E^*), i.e. the energy which the plasma would have in a coil without end losses.

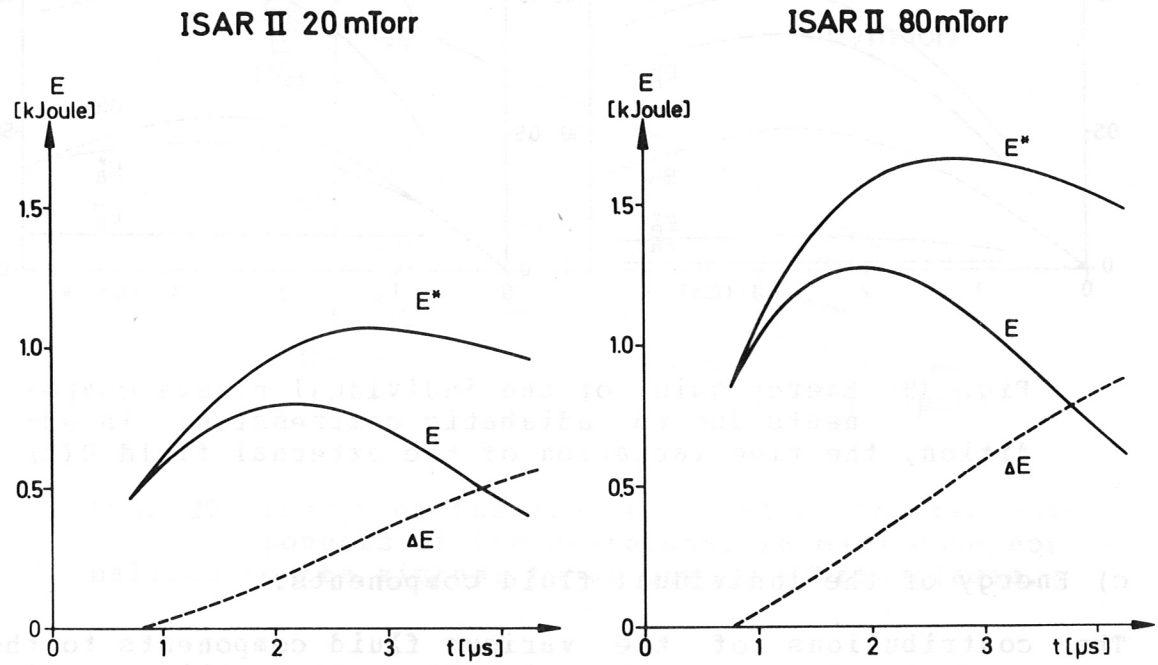

Fig. 18 Total energy in the plasma E, total energy losses Δ E, and sum of the two energies E^*

b) Energy gain of the individual fluid components:

The adiabatic heating by compression due to the magnetic field was plotted for ions and electrons in Fig. 19. The starting point in each case was the energy component at the time t_o = 0.75 μsec. For reference the time variation of the external field B(t) is also plotted (dashed curve). At the filling pressure of 80 mTorr the energy gain of the

plasma is higher than in the 20 mTorr case. In the low pressure case the perpendicular component contains the bulk of the energy (compared with the other components). The parallel ion component does not undergo any change as a result of adiabatic compression in either case.

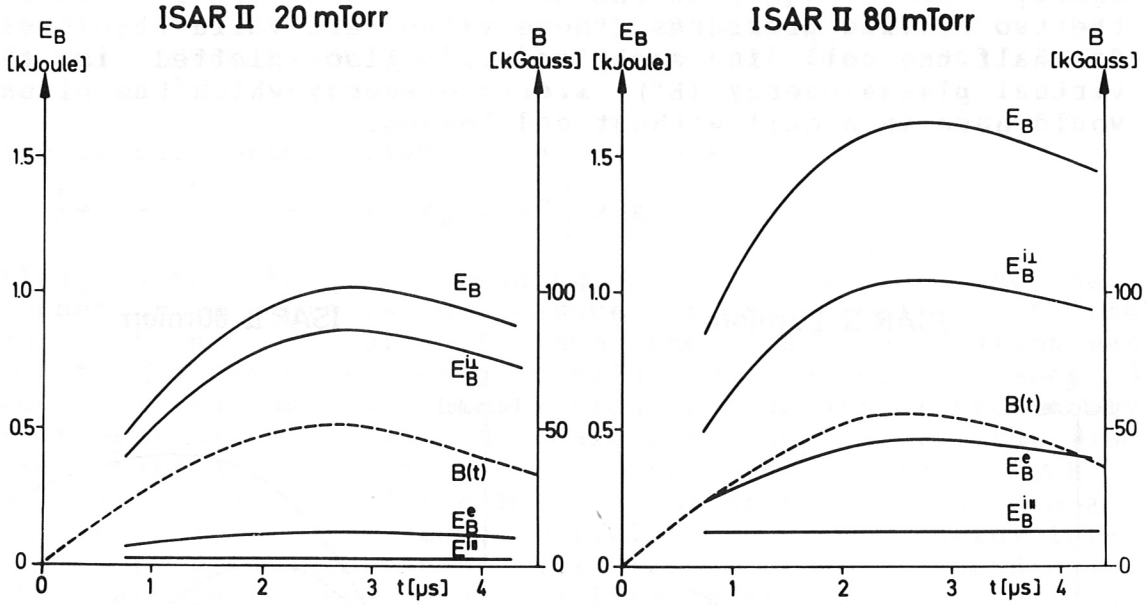

Fig. 19 Energy gain of the individual plasma components due to adiabatic compression; in addition, the time variation of the external field B(t)

c) Energy of the individual fluid components:

The contributions of the various fluid components to the energy of the plasma are shown in Fig. 20. All energies here are normalized to the virtual energy $E^* := E + \Delta E$. In the 20 mTorr case the perpendicular component of the deuterons contains the bulk of the energy. This energy dissipates only slightly into the other degrees of freedom of the ions and transfers energy to the electrons very slowly, i.e. the relaxation is weak (see also Fig. 16). With a filling pressure of 80 mTorr, on the other hand, i.e. with stronger relaxation (see Fig. 17), the energies of the various components equalize much faster.

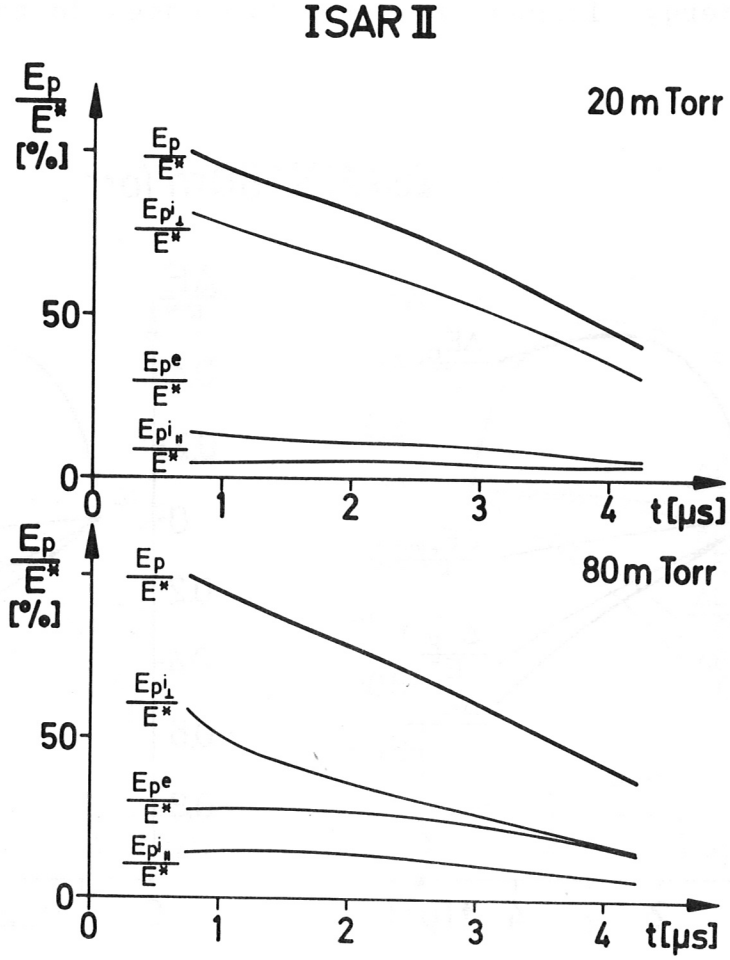

Fig. 20 Energy of the electrons and of the two components of the deuterons, in each case normalized to the virtual total energy of the plasma.

d) Energy losses classified according to the loss mechanism:

The contribution of the various processes to the energy loss are quantitatively analyzed by plotting the energy losses due to kinetic energy ΔE_{kin}, convection (pressure transport) ΔE_p, and thermal conduction ΔE_λ in Fig. 21 for the 80 mTorr case. Also shown are the sum of all energy losses ΔE and, for comparison, the energy gain due to adiabatic compression ΔE_B. Again, all energies are normalized to $E^* := E + \Delta E$. The main contribution to the energy losses at the ends is made by convection. The energy losses due to thermal conduction (through the end planes) are much smaller. The diagram on the left side of the figure shows the energy balance of the calculation without thermal conduction ($\lambda = 0$). The end points of these curves are

marked in the right-hand diagram. The convection losses thus increase when thermal conduction is cut off, and so the total energy losses in the two cases do not essentially differ.

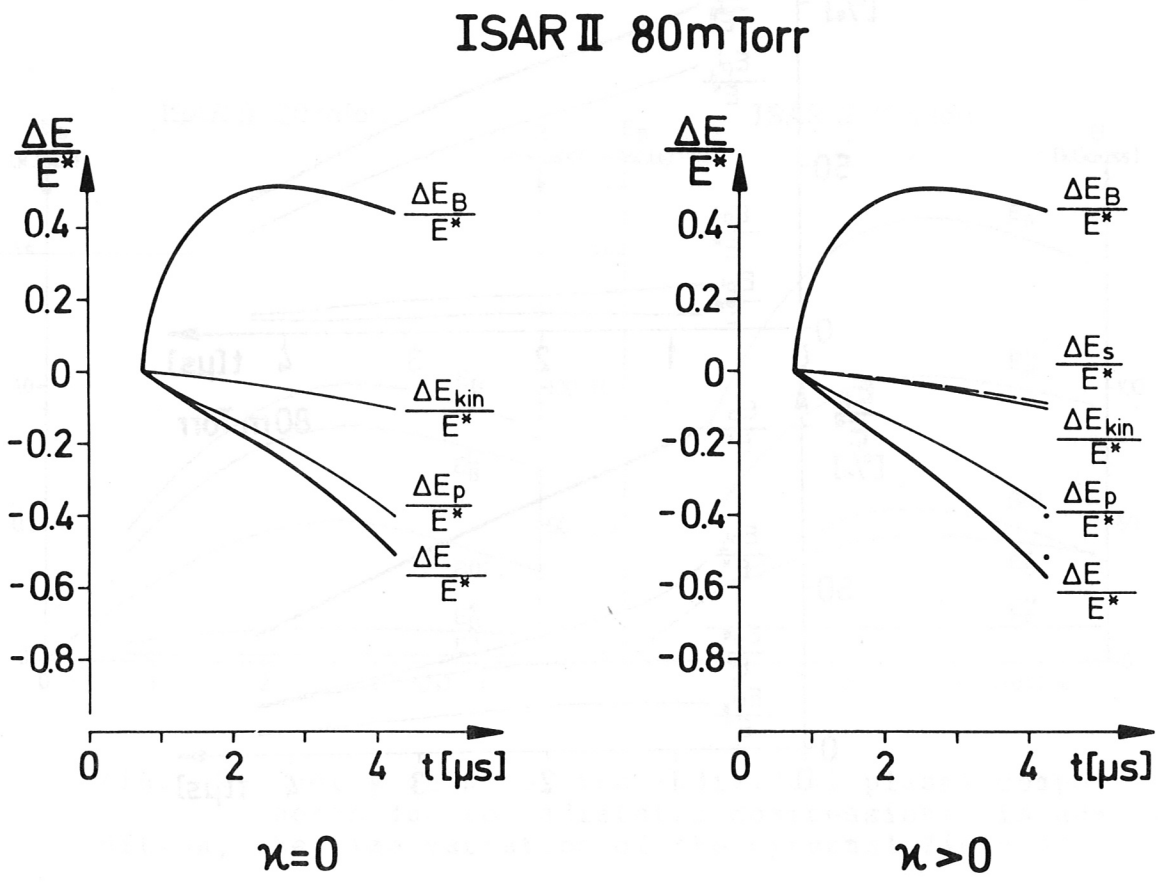

Fig. 21 Energy gain of the plasma due to adiabatic compression ΔE_B and various energy losses ΔE for the case without ($\varkappa = 0$) and with ($\varkappa > 0$) thermal conduction (80 mTorr filling pressure).

This behaviour also occurred qualitatively for the high temperature case, i.e. thermal conduction has a stronger bearing. Fig. 22 shows the same energies for the 20 mTorr case, the temperatures here being much higher.

The conclusion that the bulk of the energy losses at the end of the coil is not due to thermal conduction but to convection contradicts the results of other investigations /38/. The relation between end losses and temperature in the coil centre is discussed in section 4.3 . The diagram on the right-hand side of Fig. 22 also shows the estimated radiation losses. The scale for this curve is a factor of 10 as large as that for the other losses. This estimate

justifies ignoring the radiation losses in the energy balance in the cases discussed here.

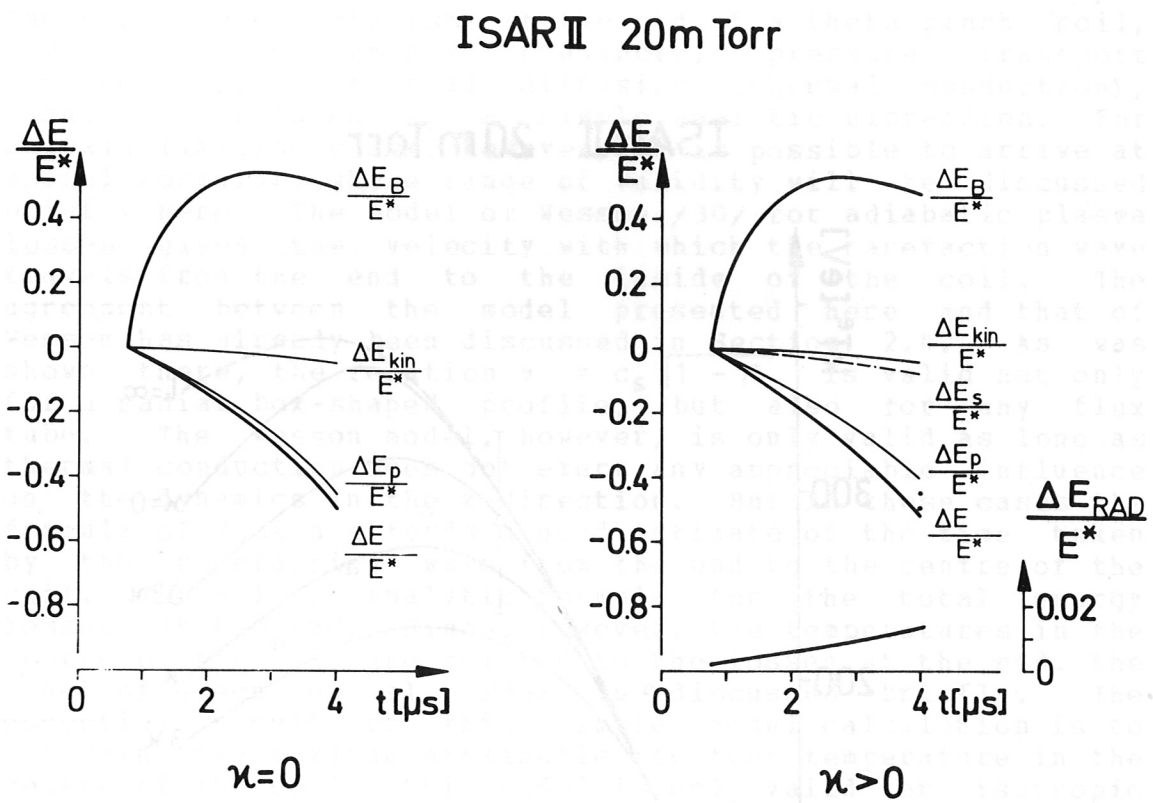

Fig. 22 Energy gain of the plasma due to adiabatic compression ΔE_B and various energy losses ΔE for the case without ($\varkappa = 0$) and with ($\varkappa > 0$) thermal conduction (20 mTorr filling pressure).

4.3 Influence of heat conduction on the axial dynamics

As has already been discussed in connection with the energy balance, thermal conduction plays only a minor part in the direct energy loss at the end. As regards the energy transport inside the coil, however, thermal conduction is of major importance. Owing to the partially very fast thermal diffusion the plasma in the centre of the coil senses the lower temperatures at the end long before the rarefaction wave coming from the end reaches the coil centre. In order to illustrate this effect, the programme was used for the same parameters, once with thermal conduction, then without thermal conduction ($\varkappa = 0$), and finally for a plasma of infinite extent ($L = \infty$). The electron temperatures in the

centre of the coil are plotted versus time in Fig. 23. The corresponding experimental values for the electron temperature are also included in this Figure for comparison. In addition, the electron temperatures resulting from a further variation of $\varkappa$, namely $\varkappa^* = (0.3 \text{ or } 3) \times \varkappa$, are plotted.

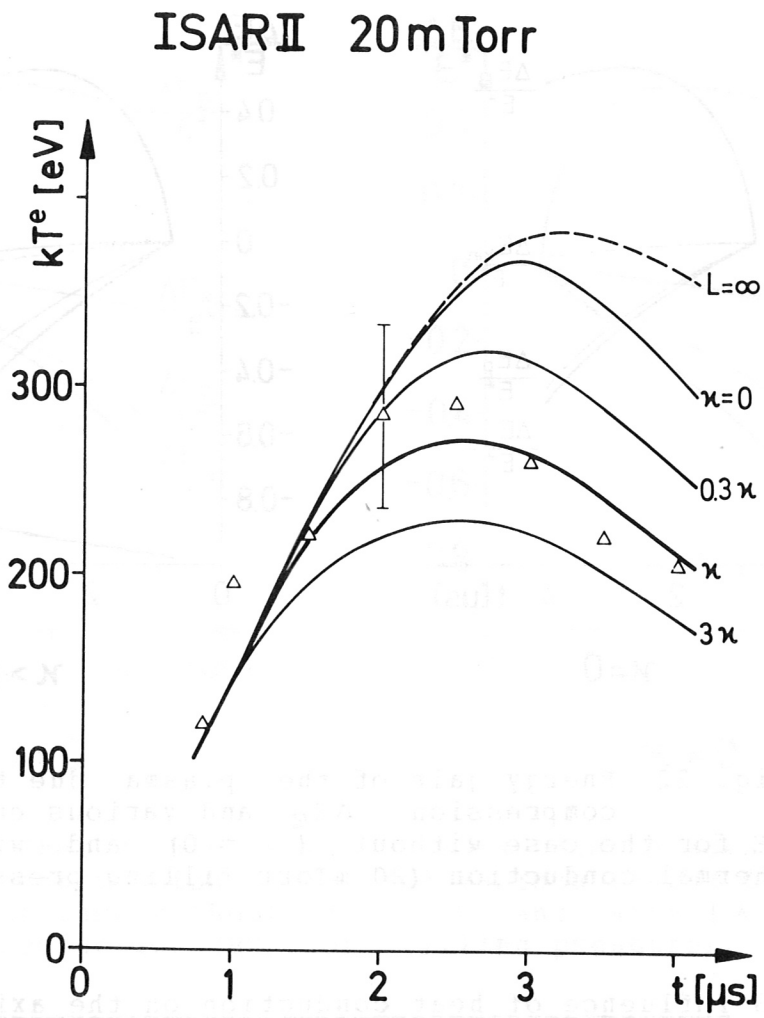

Fig. 23 Time evolution of the electron temperature in the coil centre for various thermal conductivity coefficients ($\varkappa^* = 0, (0.3, 1, 3) \times \varkappa$) and infinitely long coil ($L = \infty$) .
(△ measured values).

The much discussed question whether the coeffients used for the thermal conduction correctly describe the thermal fluxes in the plasma can only be answered positively within limits. The experimental accuracy does not allow any more

precise information than that the coefficient of the thermal conductivity of the electrons is correct to a factor of 2 - 3.

4.4 General remarks on the energy loss mechanisms

The three loss mechanisms at the end of a theta pinch coil, viz. kinetic energy transport, pressure transport (convection), and thermal diffusion (thermal conduction), cannot be related by a simple analytic expression. For certain limiting cases, however, it is possible to arrive at useful formulae, whose range of validity will be discussed briefly here. The model of Wesson /30/ for adiabatic plasma losses gives the velocity with which the rarefaction wave travels from the end to the inside of the coil. The agreement between the model presented here and that of Wesson has already been discussed in Section 2.4. As was shown there, the relation $v = c_s \sqrt{1 - \beta}$ is valid not only for a radial box-shaped profile, but also for any flux tube. The Wesson model, however, is only valid as long as thermal conduction does not exert any appreciable influence on the dynamics in the z-direction. But in these cases the formula of Wesson affords a good estimate of the time taken by the rarefaction wave from the end to the centre of the coil. There is no analytic formula for the total energy losses at the end. Since, however, the temperatures in the centre of the coil are related to the losses at the end, the model of Green et al. /38/ is discussed briefly. The essential result of this simple model calculation is to determine the maximum attainable electron temperature in the centre of the coil. This model is only valid for isotropic plasma with equal electron and ion temperatures; allowance is made only for the thermal conduction as loss mechanism and adiabatic heating as energy input. The maximum electron temperatures predicted by this model were compared with a number of results obtained with the 2D code. Although it was demonstrated here that convection is mainly responsible for the energy losses at the end of the coil, the predictions of Green et al. agree with the 2D calculations, but only within about 30 %. Surprisingly, there was even rough agreement for anisotropic plasma. This result may justify using Green's formula to obtain an estimate which may be useful at least as a basis for discussion.

4.5 Anisotropy relaxation - mirror instabilities

The calculations had not been compared hitherto with direct measurements of the perpendicular and parallel components of the deuterons because such measurements were not possible in the ISAR II experiments. In ISAR I, however, J.Neuhauser /39/ has conducted extensive investigations on the ion energy. The experiments on ISAR I were therefore enlisted

in this special connection. Figure 24 shows a comparison of the measured ion energies with the corresponding calculations. When the classical relaxation coefficients /23/ were used, the calculation (dashed curves) yielded slower relaxation than the experiment. The diamagnetic signal in the bottom diagram also shows a corresponding discrepancy between measurement and calculation (again the dashed curve). As already intimated in Section 3.3, the faster relaxation in these parameter ranges can be ascribed to the presence of mirror instabilities /40/.

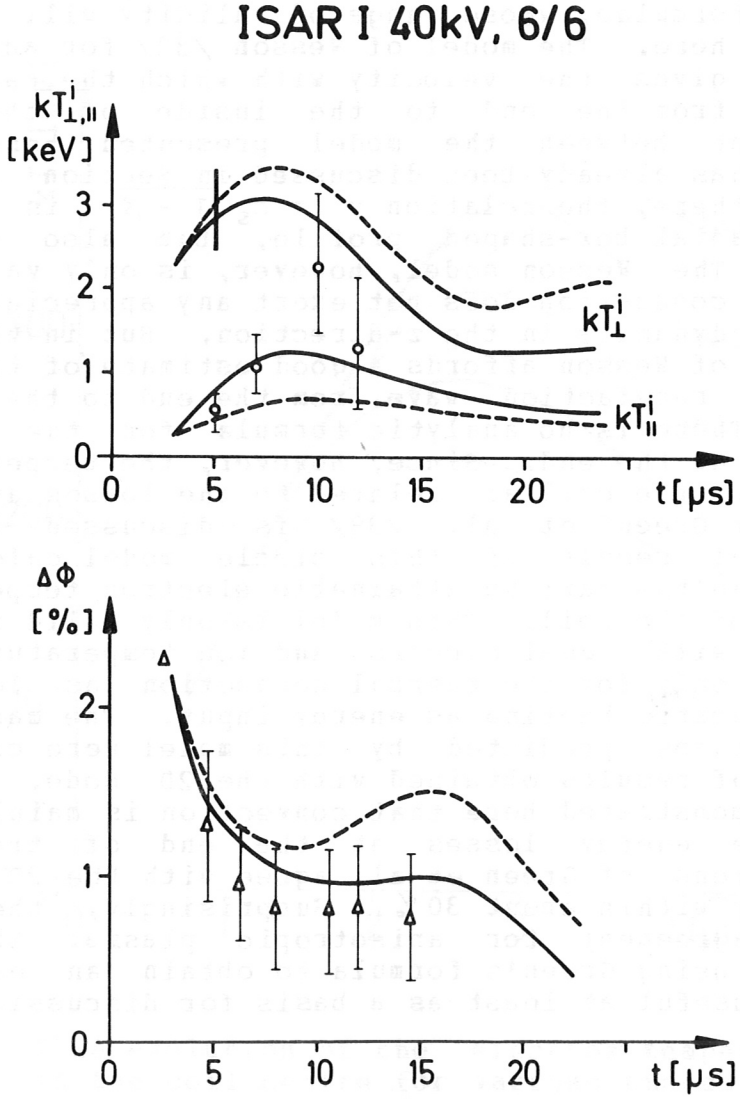

Fig. 24 Perpendicular and parallel temperatures of the deuterons and diamagnetic signal. The solid curves were calculated with additional relaxation (mirror instabilities), the dashed curves with normal relaxation (binary collisions only).

After an additional phenomenological relaxation (τ_{ii} - relaxation time of the anisotropic ions)

$$1/\tau_{ii}^{*} = 1/f_1 + 1/f_2$$

$f_1 \ldots \tau_{ii}$ (classical: binary collisions)

$$f_2 = 5 \times 10^{-6} \left(kT_{\perp}^{i}\,[eV] \right)^{-1/2}$$

had been included, the temperatures and the diamagnetic signal which are represented in Fig. 24 by solid curves were obtained. The calcualtion has thus been shown to be in satisfactory agreement with the measurement as regards these parameters. Figure 25 shows that the good agreement of the other plasma parameters is ensured by this treatment of the model.

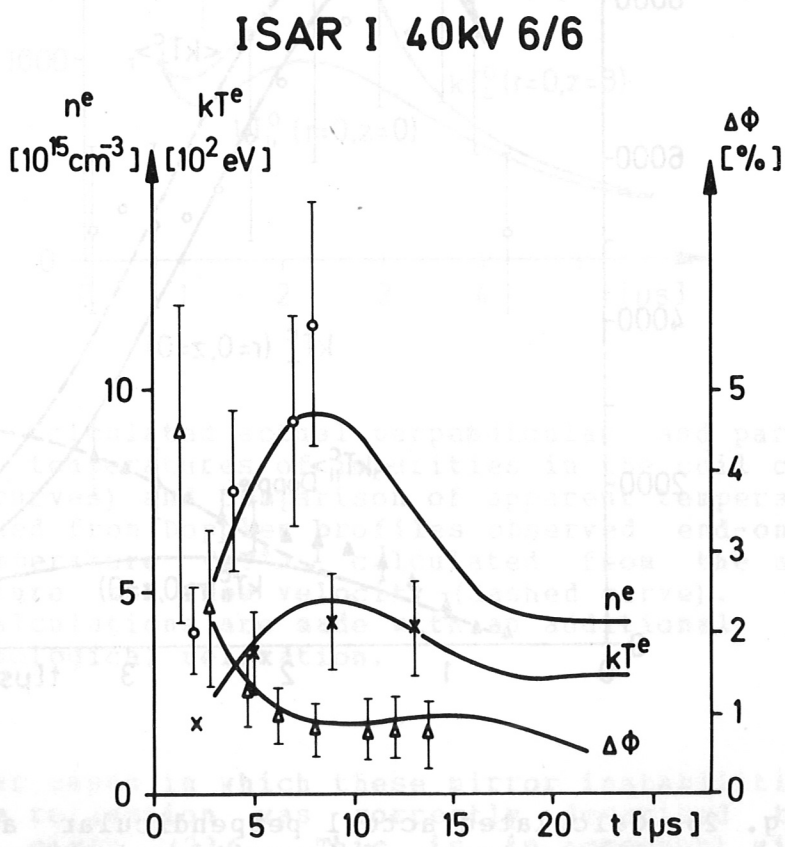

Fig. 25 Comparison of the measured electron temperature kT^e (×), electron density n^e (O), and diamagnetic signal $\Delta\phi$ (Δ) with results of the 2D code (curves).

The calculations for ISAR II (filling pressure 20 mTorr) were then made with this additional relaxation. The results for the impurity temperatures (CV and OVII) are shown in Figs. 26 and 27. It is true that the calculation and measurement are still not in optimum agreement, but compared with the corresponding Figs. 14 and 15 there is an obvious approximation of the calculated results to the temperatures actually present.

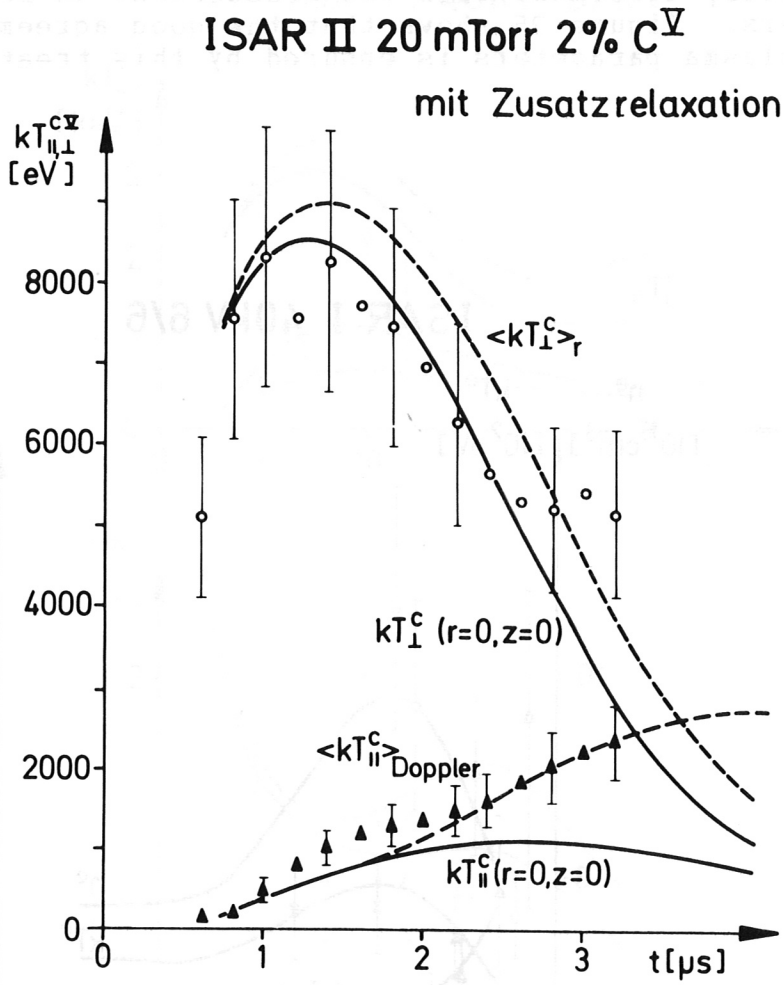

Fig. 26 Calculated actual perpendicular and parallel temperatures of impurities in the coil centre (solid curves) and comparison of apparent temperatures determined from Doppler profiles observed end-on (▲) and side-on (o) with temperatures $\langle kT^c \rangle$ calculated from the actual temperatures and flow velocity (dashed curve). These calculations are made with an additional phenomenological relaxation.

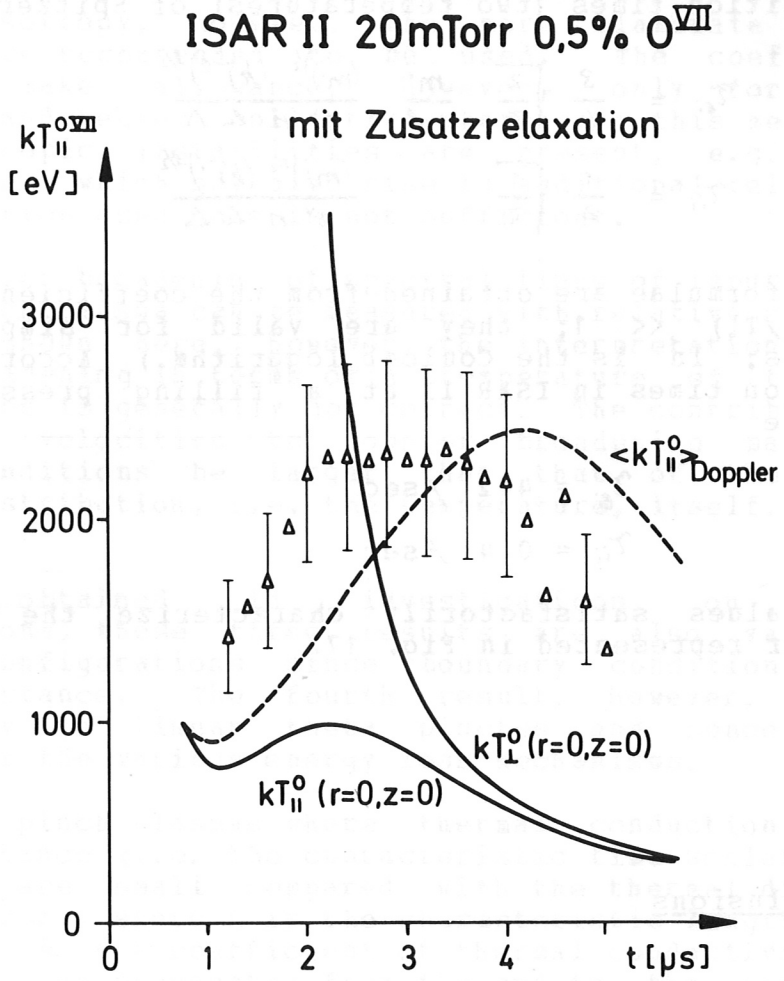

Fig. 27 Calculated actual perpendicular and parallel temperatures of impurities in the coil centre (solid curves) and comparison of apparent temperatures determined from Doppler profiles observed end-on (Δ) with temperature <kT°> calculated from the actual temperature and flow velocity (dashed curve). These calculations are made with an additional phenomenological relaxation.

In all other cases in which these mirror instabilities did not occur the relaxation was correctly described by the coefficients given /23/. This is in agreement with the result of the investigations conducted by Andelfinger et al. /41/.

For the limiting case of weak anisotropy the formulae of Chodura-Pohl /23/ are simplified; the resulting relaxation

times agree to within a numerical factor with the equipartition times (two temperatures) of Spitzer /5/ :

$$\tau_{ei} = \frac{3}{16}\sqrt{\frac{2}{\pi}}\,\frac{m^i}{m^e}\,\frac{(m^i)^{1/2}\,(k\bar{T}^e)^{3/2}}{e^4\, n\, \ln\Lambda}$$

$$\tau_{ii} = \frac{1}{2}\sqrt{\frac{1}{\pi}}\,\frac{(m^i)^{1/2}\,(k\bar{T}^i)^{3/2}}{e^4\, n\, \ln\Lambda}$$

(These formulae are obtained from the coefficients /23/ for $(1 - T_\perp^i/T_\parallel^i) \ll 1$; they are valid for simply ionized particles; ln is the Coulomb logarithm.) Accordingly, the relaxation times in ISAR II at a filling pressure of 80 mTorr are

$$\tau_{ei} = 4.2\ \mu\text{sec}$$

$$\tau_{ii} = 0.4\ \mu\text{sec}$$

These values satisfactorily characterize the temperature behaviour represented in Fig. 17.

5. Conclusions

A computer experiment such as was presented here by means of the results of a 2D MHD programme for theta pinch discharges is a useful tool for interpreting physical phenomena; it also allows predictions about theta pinch experiments.

The essential results of the foregoing investigations, in which measurements and calculations were in close coordination, are briefly as follows:

1) The adiabatic compression is the dominant heating mechanism in theta pinch discharges after the early implosion phase; the contribution by ohmic heating in these late phases can therefore be treated with the known analytical formulae for adiabatic heating, this being of importance for the otherwise complex investigations in toroidal configurations.

2) The relaxation of the anisotropic ions, which are always present in fast compression experiments, is properly described by the coefficients of Chodura-Pohl /23/ or Lehner /25/. In the limiting case of weak anisotropy these coefficients transform to the formulae of Spitzer /5/ up to a numerical factor, and so for rough estimates these

somewhat simpler formulae can be used in many cases. For strong anisotropy, however, the more elaborate formulae mentioned are recommended to be used. The coefficients mentioned make allowance, however, only for binary collisions and neglect collective phenomena; this means that when microscopic instabilities are present, e.g. mirror instabilities, which may give rise to additional relaxation, the description used here is not sufficient.

3) The Doppler broadening of spectral lines of impurity ions in a deuteron plasma can be measured with relative ease. As has been shown here, however, the interpretation of this Doppler broadening in terms of a temperature of the line emitting ions is generally not correct. The contribution of macroscopic velocities to Doppler broadening may under certain conditions be larger than that of the random velocity distribution, i.e. the temperature, itself.

Although obtained in investigations on linear configurations, these three results are also valid for toroidal configurations since boundary conditions are of minor importance. The fourth result, however, applies specifically to linear theta pinches and concerns the influence of the various energy loss mechanisms.

4) In theta pinch plasmas where thermal conduction is of minor importance (i.e. the characteristic time scales of the experiment are small compared with the thermal diffusion time $t = L^2/\varkappa$, where L is the characteristic length of the experiment, $\varkappa$ the coefficient of thermal conductivity) the rarefaction wave propagates from the end to the centre of the coil with a velocity $v = c_s (1 - \beta)^{1/2}$ /30/. (Here the the velocity of sound c_s and the plasma beta β are functions of space and time.) For such plasmas this analytic formulae is a useful tool for estimating the arrival of the rarefaction wave at the centre of the coil. In the case of plasmas whose dynamics are strongly affected by thermal conduction the foregoing is, however, no longer valid. A rough estimate of Green et al. /38/ that takes into account only the energy losses due to thermal conduction yields approximately the same maximum attainable electron temperatures in the centre of the coil as the relatively complex calculations used here. A detailed energy balance in the model described here showed that the main part of the energy transport through the end plane of the coil is due to convection, this being true in all the cases investigated (i.e. irrespective of whether the thermal diffusion times were small or large compared with the discharge time). In high temperature plasmas the thermal conduction is of prime importance for the energy transport inside the coil; the result of this thermal diffusion is that axial temperature profiles disappear fast and hence the maximum temperatures in the centre of the coil may be appreciably lowered under certain conditions.

Symbols

kT	$[\ eV\ ]$	temperature
n	$[\ cm^{-3}\ ]$	particle density
$\varrho = m\,n$	$[\ g/cm^3\ ]$	mass density
V	$[\ cm/sec\ ]$	macroscopic velocity
$\vec{\vec{P}}^e = n\,kT^e\,\delta^\nu_\mu = p^e\,\delta^\nu_\mu$		electron pressure (isotropic)
$\vec{\vec{P}}^i = \begin{pmatrix} p^i_\perp & 0 & 0 \\ 0 & p^i_\perp & 0 \\ 0 & 0 & p^i_\parallel \end{pmatrix}$		ion pressure (anisotropic)
$\vec{\vec{P}} = \vec{\vec{P}}^e + \vec{\vec{P}}^i$		total pressure
$\vec{B} = (B_r, 0, B_z)$	$[\text{Gauss}]$	magnetic field
$\vec{j}$		current density
$\vec{E}$		electric field
J^{ie}_μ , $J^{ei}_{\alpha\alpha}$, ..etc.		collision terms
$S^e_\alpha = m^e \int f(w)\ (w-v)_\alpha (w-v)^2\ d\,w$		heat flux (electrons)
$S^{i_\perp}_\alpha = \frac{1}{2} m^i \int f(w)\ (w-v)_\alpha (w-v)^2_\perp\ d^3w$		heat flux (ions $\perp$)
$S^{i_\parallel}_\alpha = m^i \int f(w)\ (w-v)_\alpha (w-v)^2_\perp\ d^3w$		heat flux (ions $\parallel$)
$F(r,z,t) = \int_0^r B_z\, r'\, dr' = \frac{1}{2} s^2$		magnetic flux
R_B	$[\ cm\ ]$	plasma radius
R_C	$[\ cm\ ]$	coil radius
L	$[\ cm\ ]$	coil length

$N = 2\pi \int_0^{R_B} n\, r\, dr$ [cm^{-1}] line density

$\phi_S = 2\pi \int_0^{R_B} (B_a - B_i)\, r\, dr$ diamagnetic signal

$\Delta\phi = \phi_S / \pi B_a R_c^2$ [%] displaced flux

$\dot{N}$ [neutrons/sec] neutron flux

$r_{1/2}$ [cm] half-radius of n(r)

$\beta = (p^e + p_i^i) / (B_a^2/8\pi)$ plasma beta

B_a external magnetic field

$B_i(r)$ field within the plasma

ε emission coefficient

λ_o' [Å] wavelength of line radiation

$\lambda_o = \lambda_o' (1 - V/c)$ Doppler shifted wavelength

$\lambda_D = \left(\frac{2kT_i^s}{m^s c^2} \lambda_o'^2 \right)^{1/2}$ Doppler wavelength

$P(\lambda)$ [Watt/sterad Å] radiation power

Energies:

$E = E_{kin} + E_p$ energy within the plasma

$$E_{kin} = 2\pi \int_0^{L} \int_0^{R_B} \left[\tfrac{1}{2} \rho v^2 \right]_{t=t_1} r\, dr\, dz = 2\pi \int_0^{L} \int_0^{R_B} \left[\tfrac{1}{2} \rho^e v^2 + \tfrac{1}{2} \rho^i v^2 \right]_{t=t_1} r\, dr\, dz$$

$$E_p = 2\pi \int_0^{L} \int_0^{R_B} \left[\tfrac{3}{2} p^e + p_\perp^i + \tfrac{1}{2} p_\parallel^i \right]_{t=t_1} r\, dr\, dz$$

$E_{kin} = E_{kin}^e + E_{kin}^i$ kinetic energy

$E_p = E_p^e + E_p^{i_\perp} + E_p^{i_\parallel}$ internal energy

$$\Delta E = \Delta E_{kin} + \Delta E_p + \Delta E_S \qquad \text{energy losses}$$

$$\Delta E_{kin} = 2\pi \int_{t_0}^{t_1} \int_{0}^{R_E} \left[\left(\frac{1}{2} \rho v^2 \right) v \right]_{z=L} r \, dr \, dt$$

$$\Delta E_p = 2\pi \int_{t_0}^{t_1} \int_{0}^{R_E} \left[\left(\frac{5}{2} p^e + p_\perp^i + \frac{3}{2} p_\parallel^i \right) v \right]_{z=L} r \, dr \, dt$$

$$\Delta E_S = 2\pi \int_{t_0}^{t_1} \int_{0}^{R_E} \left[\frac{3}{2} S_z^e + S_z^{i_\perp} + \frac{1}{2} S_z^{i_\parallel} \right]_{z=L} r \, dr \, dt$$

$\Delta E_{kin} = \Delta E_{kin}^e + \Delta E_{kin}^i$ kinetic energy losses

$\Delta E_p = \Delta E_p^e + \Delta E_p^{i_\perp} + \Delta E_p^{i_\parallel}$ losses due to convection

$\Delta E_S = \Delta E_S^e + \Delta E_S^{i_\perp} + \Delta E_S^{i_\parallel}$ losses due to heat conduction

$$\Delta E_E = 2\pi \int_{t_0}^{t_1} \int_{0}^{L} \int_{0}^{R_E} (p^e + p_\perp^i) \, \mathrm{DIVW} \; r \, dr \, dz \, dt$$

energy gain due to magnetic field compression

$\Delta E_E = \Delta E_E^e + \Delta E_E^{i_\perp}$ $\quad (\Delta E_E^{i_\parallel} = 0)$

$E_E = E(t=t_0) + \Delta E_R$

$E^* := E + \Delta E$ energy if no losses present

$\delta E = \left[E(t_0) + \Delta E_E - E^* \right] / E^*$ measure for energy conservation

ΔE_{Rad} energy losses due to radiation

References:

/ 1/ M.ROSENBLUTH: "Dynamics of a Pinched Gas", Sct. 1 in 'Magnetohydrodynamics' by R.K.M.Landshoff, Stanford University Press, Stanford, 1957

/ 2/ H.KEVER: "Zur Theorie der magnetischen Kompression zylindersymmetrischer Plasmen", Laboratory Report JUL-2-PP, Kernforschungsanlage Jűlich, (1960)

/ 3/ K.BOYER,W.C.ELMORE,E.M.LITTLE,W.E.QUINN and J.L.TUCK: "Studies of Plasma Heated in a Fast-rising Axial Magnetic Field (SCYLLA)", Phys. Rev. 119,831 (1960)

/ 4/ R.WILHELM: "Die Energieaufnahme der Ionen in einem sehr schnellen Theta-Pinch", Z.Physik 222, 208-221 (1969)

/ 5/ L.SPITZER,Jr.: "Physics of Fully Ionized Gases", Interscience Publishers, New York-London, 1962

/ 6/ R.Z.SAGDEEV: Proc. Symp. in App. Maths. (April 1965), American Math. Soc. XVIII p.281 (1967);
R.Z.SAGDEEV,A.A.GALEEV: I.A.E.A. Report IC/66/64 Trieste (1966)

/ 7/ H.A.B.BODIN,J.McCARTAN,A.A.NEWTON and G.WOLF: Diffusion and Stability of high- Plasma in an 8 Metre Theta Pinch", Third I.A.E.A. Conference on Plasma Physics and Controlled Fusion Research, Novosibirsk, (1968)

/ 8/ D.DŰCHS: "Untersuchungen űber den Einfluss von Neutralgas auf die Dynamik der Theta-Pinch-Entladungen", Laboratory Report IPP 1/14, IPP 6/10 (1963)

/ 9/ D.FISHER; Culham Reports ('Radial Version of the 1D-MHD Code')

/10/ H.FISSER: "Numerical Solutions of the Magneto-hydrodynamic Equations for One-Dimensional Theta-Pinch Geometry", 'First European Confererence on Controlled Fusion and Plasma Physics', Műnchen 1966

/11/ G.HAIN,K.HAIN,W.KŐPPENDŐRFER,K.V.ROBERTS,S.J.ROBERTS: "Fully Ionized Pinch Collapse", Zeitschr. Natur., Bd. 15a, 1039-1050 (1960)

/12/ R.CHODURA: "Numerical Investigations of Collisionless Compression of a Plasma with Anomalous Friction", The Physics of Fluids, Vol 11, Nr. 2, p. 400-407, 1968

/13/ D.FISHER; Culham Reports ('Axial Version of the 1D-MHD Code')

/14/ W.B.JONES,L.M.GOLDMAN,R.W.KILB,R.L.BINGHAM: "Energy and Particle Loss from a Short Theta Pinch", Phys.Fluids 13,800-809, (1970)

/15/ W.SCHNEIDER: "One-Dimensional MHD Calculations of the Axial Behaviour of a Theta Pinch Plasma", IPP Laboratory Report under preparation

/16/ R.L.MORSE: "Methods in Computational Physics", Vol. 9, 213, Academic Press (1970)

/17/ D.BISKAMP,R.CHODURA: "Computer Simulation of Anomalous Resistance", Fourth I.A.E.A. Conference on Plasma Physics and Controlled Fusion Research, Madison(Wisconsin), (1971)

/18/ R.CHODURA K.Graf Finck v. FINCKENSTEIN: "Vlasov Description of a Supercritical Magneto-acoustic Compression Pulse", Laboratory Report IPP 1/113, 6/92 (1970)

/19/ K.V.ROBERTS,F.HERTWECK,S.J.ROBERTS: "Thetatron, a Two-Dimensional Magnetohydrodynamic Computer Programme", Laboratory Report CLM-R 29, Culham, 1963

/20/ A.SCHLÜTER: "Dynamik des Plasmas", Z.Natur. 5,72 (1950)

/21/ S.CHAPMAN,T.G.COWLING: "The Mathematical Theory of Non-Uniform Gases", University Press, Cambridge,1964

/22/ F.HERTWECK: "Allgemeine 13-Momenten-Näherung zur Fokker-Planck-Gleichung eines Plasmas", Laboratory Report IPP 6/1 (1962)

/23/ R.CHODURA,F.POHL: "Hydromagnetic Equations for Anisotropic Plasmas including Transport Coefficients", Laboratory Report IPP 1/112 (1970)

/24/ V.J.KOGAN: "Plasma Physics and the Problem of Controlled Thermonuclear Reactions", M.A.Leontovich Ed., Pergamon Press, New York, Vol.1 (1961)

/25/ G.LEHNER: "On the Relaxation of Anisotropic Plasmas", Zeitschrift f. Physik 206, 284-292, (1967)

/26/ R.D.RICHTMYER,K.W.MORTON: "Difference Methods for Initial-Value Problems", Interscience Publishers (John Wiley Sons,inc.), New York-London-Sydney,1967

/27/ W.SCHNEIDER: "2D(r,z) MHD-Code", IPP Laboratory Report under preparation

/28/ G.LEHNER,J.NEUHAUSER,F.POHL: private communication, a simple numerical model for the relaxation of anisotropic plasmas; based on /25/

/29/ G.LEHNER,F.POHL: "The Relaxation of Heavy Ion Impurities in an Anisotropic Deuterium Plasma", Laboratory Report IPP 1/91 (1968)

/30/ J.B.TAYLOR,J.A.WESSON: "End Losses from a Theta Pinch", Nuclear Fusion 5, 159-161 (1965)

/31/ W.BRAUN,M.KAUFMANN,H.RÖHR,W.SCHNEIDER: "Diffusion eines stossfreien und stossbehafteten Plasmas", Frühjahrstagung der DPG, München, (1970)

/32/ W.ENGELHARDT,W.KÖPPENDÖRFER,M.MÜNICH,J.SOMMER: IPP Laboratory Report under preparation

/33/ T.S.GREEN: "An Investigation of the Theta Pinch using Magnetic Pick-up Loops", Nuclear Fusion 2, 92 (1962)

/34/ R.F.POST: "Controlled Fusion Research.- An Application of the Physics of High-Temperature Plasmas", Rev.Modern Phys. 28, 338 (1956)

/35/ Hans R.GRIEM: "Plasma Spectroscopy", McGraw Hill (1964)

/36/ H.-J.KUNZE,A.H.GABRIEL and Hans R.GRIEM: "Measurements of Collisional Rate Coefficients for Helium-like Carbon Ions in a Plasma", The Physical Review, Vol.165, No.1, p.267-276 (1968)

/37/ P.BOGEN,Y.T.LIE,D.RUSBÜLDT and J.SCHLÜTER: "Relaxation of Ion Pressure Anisotropy and Energy Transfer between Ions and Electrons in High Density Plasmas", Conference on Plasma Physics and Controlled Nuclear Fusion Research, Novosibirsk; Proceedings (1968)

/38/ T.S.GREEN,D.L.FISHER,A.H.GABRIEL,I.J.MORGAN,A.A.NEWTON: "Energy loss from a Theta Pinch", Phys. Fluids 10, 1663-1675 (1967)

/39/ J.NEUHAUSER: "Geschwindigkeitsverteilung anisotroper Deuteriumsplasmen aus zeitaufgelösten Neutronenspektren", Laboratory Report IPP 1/109 (1970)

/40/ M.KAUFMANN,J.NEUHAUSER,H.RÖHR: "Experimental Proof of Mirror Instabilities in the ISAR I Theta Pinch", Z.Physik 244, 99-216 (1971)

/41/ C.ANDELFINGER,E.FÜNFER,G.LEHNER,H.PARETZKE,F.POHL, U.SEIDEL,K.J.SOMMER und U.ULRICH: "Untersuchungen zur Anisotropie und Relaxation des Plasmas am ISAR I -Mega-joule-Thetapinch" , Laboratory Report IPP 1/67 (1967)